UDC 532.52.011/.08:
621.452.32

TECHNICAL REPORT OF NATIONAL AEROSPACE LABORATORY

TR-378T

Three-Dimensional Flow Field Due to a Radial Vortex and Source Line Spanning an Annulus

Atsuhiro TAMURA

August 1974

NATIONAL AEROSPACE LABORATORY

CHŌFU, TOKYO, JAPAN

Three-Dimensional Flow Field Due to a Radial Vortex and Source Line Spanning an Annulus*

By Atsuhiro TAMURA**

ABSTRACT

A theoretical investigation of the three dimensional potential flow field due to a radial vortex and source line spanning an annulus is carried out in this paper. The three dimensional effects due to finite radius hub and annulus walls are found to be appreciable, especially for a low hub/tip ratio configuration. The discrepancy between the two and three dimensional solutions are found to be large near the hub, moderate at the tip and negligibly small at the mid radius.

概　　要

円環状断面を有する直線ダクト内に置かれた半径方間渦線ならびに吹出し線によって誘導される三次元渦無し流れ場を理論的に解析し，円環の内外径比が三次元流れ場におよぼす影響を半径比0.6および0.3の場合について求め二次元理論と比較した。二次元理論との相違は，半径比が1より小さくなるに従って次第に大きくなり，ことに内壁ではかなりの差を示している，又外壁に近い側は中程度で中間半径では二次元，三次元理論の差はほとんど無視できる程度であった。

1. INTRODUCTION

In several practical situations involving internal flow, the flow field due to a body spanning an annulus is of interest. Some of the examples are; (a) A strut of either cylindrical, ellipsoidal or aerofoil section spanning an annulus used in various aircraft, marine and industrial power plants and propulsion machinery. (b) The flow around the blades (rotating or stationary) of turbomachinery. The hub and annulus walls impose additional constraint on the flow and introduces three dimensionality in the flow field. One of the basic building blocks for the eventual solution of the flow field is the understanding of the flow field due to a vortex, source or sink line spanning an annulus with finite hub tip ratio. This is the objective of this paper. It is hoped that a good understanding of this flow field would lead to the development of a three dimensional singularity method for analyzing the flow around streamlined bodies spanning an annulus.

One of the early investigations of this flow is due to Tyson[2] who evaluated the flow field due to a radial vortex line of constant strength spanning an annulus of hub/tip ratio of 0.6. The present author has found that the numerical values for velocities derived by Tyson are in error. Rossow[3] developed some expressions for a single radial source line spanning an annulus, but no numerical solutions were given. A unified approach, valid for both vortex and source (sink) flows, is provided in this paper. The flow field is evaluated for two values of hub/tip ratio and at various locations inside the annulus. The theory and numerical solutions are valid for incompressible, inviscid and steady irrotational flow. The strength of the vortex is constant, but the source (or sink) strength could be varying radially.

2. NOMENCLATURE

ν	Hub-to-tip ratio
R_t	Radius of the outer casing wall
R_h	Radius of the hub
θ	Angular coordinate in a cylindrical coordinate system (rad)

* Received June 4, 1974

** Aeroengine Division

η Non-dimensional radial coordinate normalized by R_t in a cylindrical coordinate system

η_{mid} Mid radius = $(1+\nu)/2$

ζ Non-dimensional axial coordinate normalized by R_t in a cylindrical coordinate system

Γ Non-dimensional strength of a radial vortex line

$Q(\eta)$ Non-dimensional strength of a radial source line

γ Strength of the spread vortex line

μ Strength of the spread source line

δ Angular width of spread vortex and source line

Φ_v Non-dimensional velocity potential due to a single radial vortex line of constant strength

Φ_s Non-dimensional velocity potential due to a single radial source line of variable strength

$u_{v\theta}, u_{v\eta}, u_{v\zeta}$ Non-dimensional tangential, radial and axial velocity components due to a single radial vortex line of constant strength

$u_{s\theta}, u_{s\eta}, u_{s\zeta}$ Non-dimensional tangential, radial and axial velocity components due to a single radial source line of variable strength

K_{mn} n-th eigenvalue referred to m-th order Bessel function

$J_m(K_{mn}\eta)$ The first kind Bessel function of m-th order

$Y_m(K_{mn}\eta)$ The second kind Bessel function of m-th order

$$Z_m(K_{mn},\eta) = J_m(K_{mn}\eta)\cdot Y_m'(K_{mn}) - J_m'(K_{mn})\cdot Y_m(K_{mn}\eta)$$

$$F_v(K_{mn},\nu) = \int_\nu^1 \eta Z_m(K_{mn}\eta)\,d\eta \Big/ \int_\nu^1 \eta Z_m^2(K_{mn}\eta)\,d\eta$$

$$F_s(K_{mn},\nu) = \int_\nu^1 Q(\eta) Z_m(K_{mn}\eta)\,d\eta \Big/ \int_\nu^1 \eta Z_m^2(K_{mn}\eta)\,d\eta$$

SUBSCRIPTS

m Refer to m-th order Bessel function

n Refer to n-th eigenvalue associated with the Bessel function of each order

v Refer to the vortex system

s Refer to the source system

3. THE BASIC THEORY

3.1 The Three-Dimensional Flow Field Due to a Single Radial Vortex Line of Constant Strength Spanning an Annulus

In order to carry out a potential flow analysis, the following basic assumtions were made: the flow is inviscid, incompressible and has no heat transfer. A single radial vortex line of constant strength Γ, located at $\zeta = 0$, $\theta = 0$, spans the annulus region between the hub and outer casing wall (see Figure 1). The theoretical work reported in this section is due to Tyson (2). The whole flow field is irrotational except for the vortex line. The irrotational and continuity conditions are reduced to a Laplace equation in terms of the velocity potential Φ_v and the independent variables θ, η, ζ (see Figure 1),

$$\nabla^2\Phi_v = \frac{1}{\eta}\frac{\partial}{\partial\eta}\left(\eta\frac{\partial\Phi_v}{\partial\eta}\right) + \frac{1}{\eta^2}\frac{\partial^2\Phi_v}{\partial\theta^2} + \frac{\partial^2\Phi_v}{\partial\zeta^2} = 0. \tag{1}$$

The boundary conditions are:

a) The axial velocity should vanish at $\zeta = \pm\infty$

$$\left(\frac{\partial\Phi_v}{\partial\zeta}\right)_{\zeta\to\pm\infty} = 0 \tag{2}$$

b) The radial velocity should vanish at hub and outer casing wall.

$$\left(\frac{\partial\Phi_v}{\partial\eta}\right)_{\eta=\nu,1} = 0 \tag{3}$$

c) The radial velocity should vanish at $\zeta = \pm\infty$

$$\left(\frac{\partial\Phi_v}{\partial\eta}\right)_{\zeta\to\pm\infty} = 0 \tag{4}$$

d) At plus and minus infinity, the distribution of the tangential velocity must be irrotational. Furthermore, the total magnitude of the circulation must be equal to the strength of the radial vortex line. For convenience, let the magnitude of the circulation around the hub on either side of the vortex line be $\Gamma/2$. These boundary conditions are the same as those of Tyson (Reference 2) but the definition of the positive direction of rotation of the vortex is based on the right-hand screw rule. The corresponding boundary condition of Reference (3) appears different from the above expression, since the initial value of the circulation upstream due to the vortex line is taken to be $-\Gamma/2$ here and zero in Reference 3. The present objective is to determine the perturbed

flow field which is induced by either vortex line or source line only. The above difference of initial circulation may easily be taken into consideration by adjusting the mean flow condition which will be superposed on the above perturbed flow. Circulation about the ζ axis is $-\Gamma/2$ at $\zeta = +\infty$ and $\Gamma/2$ at $\zeta = -\infty$; then, the tangential velocity at $\zeta = \pm\infty$ is given by the following equations:

$$\frac{1}{\eta}\left(\frac{\partial \Phi_v}{\partial \theta}\right)_{\zeta \to +\infty} = -\frac{\Gamma}{4\pi\eta} \tag{5}$$

and

$$\frac{1}{\eta}\left(\frac{\partial \Phi_v}{\partial \theta}\right)_{\zeta \to -\infty} = \frac{\Gamma}{4\pi\eta} \ . \tag{6}$$

e) The boundary conditions must be specified in the vicinity of the vortex line. The behavior of the tangential velocity close to the singular point (ζ = 0-plane) is represented by the following expression;

$$\frac{1}{\eta}\left(\frac{\partial \Phi_v}{\partial \theta}\right)_{\zeta \to \pm 0} = \begin{cases} \mp \dfrac{\Gamma}{2\eta}, & -\dfrac{\delta}{2} < \theta < \dfrac{\delta}{2} \\ 0 \ , & \dfrac{\delta}{2} < \theta < 2\pi - \dfrac{\delta}{2} \ . \end{cases} \tag{7}$$

Detailed derivation of the specification of the boundary conditions is given in Appendix A. The solution of the Laplace equation is given by the following expression:

$$\Phi_v = \sum_{m=0}^{\infty} (A_m \cos m\theta + B_m \sin m\theta) \sum_{n=1}^{\infty} (C \cdot e^{-K\zeta} + D \cdot e^{K\zeta})(a J_m(K\eta) + b Y_m(K\eta)), \tag{8}$$

where a, b, A_m, B_m, C, D, K are constants which must be determined, m, n are integer numbers and J_m, Y_m are the first and second kind of m-th order Bessel functions. From the boundary condition (a), $D = 0$ when $\zeta < 0$. and $C = 0$ when $\zeta > 0$. Without loss of generality, C and D can be taken as unity. Using boundary condition (b), substitution of Equation (8) into Equation (3) gives the following conditions:

$$a J_m'(K\nu) + b Y_m'(K\nu) = 0 \tag{9}$$

and

$$a J_m'(K) + b Y_m'(K) = 0 \tag{10}$$

where

$$J_m'(K\eta) = \frac{\partial J_m(K\eta)}{\partial \eta}, \quad Y_m'(K\eta) = \frac{\partial Y_m(K\eta)}{\partial \eta}.$$

Combining Equations (9) and (10),

$$\frac{J_m'(K_{mn})}{Y_m'(K_{mn})} = \frac{J_m'(K_{mn}\nu)}{Y_m'(K_{mn}\nu)} \tag{11}$$

Equation (11) is a relationship between the hub-to-tip ratio ν and the eigen value K_{mn}, where the subscript m refers to the m-th order Bessel function and n is the n-th eigen value for each m, ($m = 1, 2, 3, \ldots\ldots$, $n = 1, 2, 3, \ldots$). Introducing a new expression $Z_m(K_{mn}\eta)$, the last term of Equation (8) is given by the equation,

$$a J_m(K_{mn}\eta) + b Y_m(K_{mn}\eta) = \frac{a}{Y_m'(K_{mn})} Z_m(K_{mn}\eta), \tag{12}$$

where

$$Z_m(K_{mn}\eta) = J_m(K_{mn}\eta) \cdot Y_m'(K_{mn}) - J_m'(K_{mn}) \cdot Y_m(K_{mn}\eta) \cdot \tag{13}$$

Therefore, Equation (8) is reduced to the following expression:

$$\Phi_v = \sum_{m=0}^{\infty} (A_m \cos m\theta + B_m \sin m\theta) \sum_{n=1}^{\infty} \exp(\mp K_{mn}\zeta) \frac{a}{Y_m'(K_{mn})} Z_m(K_{mn}\eta) \ . \tag{14}$$

The relation A_m, B_m, and a are determined by the orthogonal characteristics of the trigonometric functions and Bessel function. In order to apply the boundary condition (e), differentiate Φ_v with respect to θ and equate it with Equation (7),

$$\left\{\frac{1}{\eta}\sum_{m=0}^{\infty} m(-A_m \sin m\theta + B_m \cos m\theta) \sum_{n=1}^{\infty} \frac{a}{Y_m'(K_{mn})} Z_m(K_{mn}\eta)\right\}_{\zeta \to \pm 0} = \begin{cases} \mp \dfrac{\Gamma}{2\eta}, & -\dfrac{\delta}{2} < \theta < \dfrac{\delta}{2} \\ 0 \ , & \dfrac{\delta}{2} < \theta < 2\pi - \dfrac{\delta}{2} \end{cases} \tag{15}$$

Multiply both sides by $(\cos m\theta + i \sin m\theta) \cdot \eta^2 Z_m(K_{m,n}\eta)$ then integrate from $-\pi$ to π for θ, and from ν to 1 for η :

$$m\pi(B_m - iA_m)\frac{a}{Y_m'(K_{mn})}\int_\nu^1 \eta Z_m^2(K_{mn}\eta)\,d\eta = \mp\frac{\gamma}{m}\sin\frac{m\delta}{2}\int_\nu^1 \eta Z_m(K_{mn}\eta)\,d\eta \,. \tag{16}$$

Taking the limit $\delta \to 0$, and holding $\delta\gamma = \Gamma$ constant, then,

$$m\pi(B_m - iA_m)\frac{a}{Y_m'(K_{mn})}\int_\nu^1 \eta Z_m^2(K_{mn}\eta)\,d\eta = \mp\frac{\Gamma}{2}\int_\nu^1 \eta Z_m(K_{mn}\eta)\,d\eta \,. \tag{17}$$

From the imaginary part,

$$A_m = 0 \,. \tag{18}$$

From the real part,

$$B_m = \frac{\Gamma}{2m\pi}, \text{ and } \frac{a}{Y_m'(K_{mn})} = \frac{\int_\nu^1 \eta Z_m(K_{mn}\eta)\,d\eta}{\int_\nu^1 \eta Z_m^2(K_{mn}\eta)\,d\eta}, \tag{19}$$

Where $m = 1, 2, 3, \ldots\ldots$

Taking into consideration the boundary condition (b), the solution of Laplace Equation (1) is given by Equation (20):

$$\Phi_v = \mp\frac{\Gamma}{4\pi}\left(\theta + 2\sum_{m=1}^{\infty}\frac{\sin m\theta}{m}\cdot \sum_{n=1}^{\infty}\exp(\mp K_{mn}\zeta)\,F_v(K_{mn},\nu)\,Z_m(K_{mn}\eta)\right), \tag{20}$$

where

$$F_v(K_{mn},\nu) = \frac{\int_\nu^1 \eta Z_m(K_{mn}\eta)\,d\eta}{\int_\nu^1 \eta Z_m^2(K_{mn}\eta)\,d\eta} \,. \tag{21}$$

Therefore, the tangential, radial, and axial velocity components are given by the following expressions:

$$u_{v\theta} = \mp\frac{\Gamma}{4\pi\eta}\left(1 + 2\sum_{m=1}^{\infty}\cos m\theta\cdot \sum_{n=1}^{\infty}\exp(\mp K_{mn}\zeta)\cdot F_v(K_{mn},\nu)\cdot Z_m(K_{mn}\eta)\right), \tag{22}$$

$$u_{vr} = \mp\frac{\Gamma}{2\pi}\sum_{m=1}^{\infty}\frac{\sin m\theta}{m}\sum_{n=1}^{\infty}\exp(\mp K_{mn}\zeta)\cdot F_v(K_{mn},\nu)\cdot \frac{\partial Z_m(K_{mn}\eta)}{\partial\eta} \tag{23}$$

and

$$u_{v\zeta} = \pm\frac{\Gamma}{2\pi}\sum_{m=1}^{\infty}\frac{\sin m\theta}{m}\sum_{n=1}^{\infty}K_{mn}\exp(\mp K_{mn}\zeta)\cdot F_v(K_{mn},\nu)\cdot Z_m(K_{mn}\eta), \tag{24}$$

where the upper and lower signs refer to $+\zeta$ and $-\zeta$ directions respectively.

3.2 The Three-Dimensional Flow Field Due to a Single Radial Source Line of Variable Strength Spanning an Annulus

The basic assumptions regarding the flow field (incompressible, inviscid and irrotational) are the same as those listed in the previous section. This section is based on Rossow's analysis (Reference 3). The mathematical model of a single radial source line is similar to that of a single radial vortex line except that the radial source line may have a variable strength along the radial direction. In the case of a single radial vortex line, if the strength of the vortex varies in the radial direction, there will be vortices shed according to Helmholtz's law. The flow field is no longer irrotational, but the flow field due to a variable strength radial source line is still irrotational. A single radial source line of variable strength $Q(\eta)$, located at $\zeta = 0$, $\theta = 0$, spans the annulus region between the hub and outer casing wall (see Figure 1). As in the previous section, the whole flow field is irrotational, and the velocity potential exists, satisfying the Laplace equation. Let the velocity potential due to a single radial source line be Φ_s. Therefore,

$$\frac{1}{\eta}\frac{\partial}{\partial\eta}\left(\eta\frac{\partial\Phi_s}{\partial\eta}\right) + \frac{1}{\eta^2}\frac{\partial^2\Phi_s}{\partial\theta^2} + \frac{\partial^2\Phi_s}{\partial\zeta^2} = 0 \,. \tag{25}$$

The boundary conditions are:

a) One-half of the mass flow due to a single radial source line goes to $\zeta = +\infty$ and the other half goes to $\zeta = -\infty$. Therefore, from the continuity relationship,

$$\pm\int_\nu^1 Q(\eta)\,d\eta/2 = \left(\frac{\partial\Phi_s}{\partial\zeta}\right)_{\zeta\to\pm\infty}\cdot\pi(1-\nu^2) \,. \tag{26}$$

b) The radial velocity should vanish at hub and outer casing wall,

$$\left(\frac{\partial\Phi_s}{\partial\eta}\right)_{\eta=1,\,\nu} = 0 \,. \tag{27}$$

c) The radial velocity should vanish at $\zeta = \pm\infty$

$$\left(\frac{\partial \Phi_s}{\partial \eta}\right)_{\zeta \to \pm\infty} = 0 \ . \tag{28}$$

d) The tangential velocity should vanish at $\zeta = \pm\infty$

$$\frac{1}{\eta}\left(\frac{\partial \Phi_s}{\partial \theta}\right)_{\zeta \to \pm\infty} = 0 \ . \tag{29}$$

e) The specification of the condition at points close to the single radial source line (ζ = 0-plane) is given by Equation (30). The detailed derivation is given in Appendix A.

$$\left(\frac{\partial \Phi_s}{\partial \zeta}\right)_{\zeta \to \pm 0} = \begin{cases} 0 \ , & \frac{\delta}{2} < \theta < 2\pi - \frac{\delta}{2} \\ \pm \frac{\mu(\eta)}{2\eta} \ , & -\frac{\delta}{2} < \theta < \frac{\delta}{2} \ , \end{cases} \tag{30}$$

where the upper and lower signs refer to $\zeta > 0$ and $\zeta < 0$ respectively. The solution of the Laplace equation under the given boundary conditions is given by the following equation, which is similar to those given in the previous section:

$$\Phi_s = \frac{1}{4\pi}\left(\pm\frac{2\zeta}{1-\nu^2}\int_\nu^1 Q(\eta)\,d\eta - \sum_{n=2}^{\infty} \exp(\mp K_{on}\zeta)\cdot \frac{F_s(K_{on},\nu)}{K_{on}}\cdot Z_o(K_{on}\eta) - 2\sum_{m=1}^{\infty}\cos m\theta \cdot \sum_{n=1}^{\infty}\exp(\mp K_{mn}\zeta)\cdot\frac{F_s(K_{mn},\nu)}{K_{mn}}\cdot Z_m(K_{mn}\eta)\right), \tag{31}$$

where

$$F_s(K_{mn},\nu)\frac{\int_\nu^1 Q(\eta) Z_m(K_{mn}\eta)\,d\eta}{\int_\nu^1 \eta Z_m^2(K_{mn}\eta)\,d\eta} \tag{32}$$

The tangential, radial and axial velocity components due to a single radial source line are given by the following expressions,

$$u_{s\theta} = \frac{1}{2\pi\eta}\sum_{m=1}^{\infty} m\sin m\theta \sum_{n=1}^{\infty}\exp(\mp K_{mn}\zeta)\cdot \frac{F_s(K_{mn},\nu)}{K_{mn}}\cdot Z_m(K_{mn}\eta), \tag{33}$$

$$u_{s\eta} = -\frac{1}{4\pi}\left(\sum_{n=2}^{\infty}\exp(\mp K_{on}\zeta)\frac{F_s(K_{on},\nu)}{K_{on}}\cdot \frac{\partial}{\partial\eta}Z_o(K_{on}\eta) + 2\sum_{m=1}^{\infty}\cos m\theta\cdot \sum_{n=1}^{\infty}\exp(\mp K_{mn}\zeta)\frac{F_s(K_{mn},\nu)}{K_{mn}}\frac{\partial}{\partial\eta}Z_m(K_{mn}\eta)\right) \tag{34}$$

and

$$u_{s\zeta} = \frac{1}{4\pi}\left(\pm\frac{2}{1-\nu^2}\int_\nu^1 Q(\eta)d\eta \pm \sum_{n=2}^{\infty}\exp(\mp K_{on}\zeta)\cdot F_s(K_{on},\nu)\cdot Z_o(K_{on}\eta) \pm 2\sum_{m=1}^{\infty}\cos m\theta\cdot \sum_{n=1}^{\infty}\exp(\mp K_{mn}\zeta)\,F_s(K_{mn},\nu)\cdot Z_m(K_{mn}\eta)\right) . \tag{35}$$

4. NUMERICAL TECHNIQUE AND SOLUTIONS

4.1 Determining of Eigen Values and Related Functions

The three-dimensional flow field due to radial vortex lines and source lines given in Equations (22) to (24), (33) to (35) includes an infinite number of eigen values $K_{m,n}$ and related functions $F_v(K_{m,n},\nu)$, $F_s(K_{m,n},\nu)$, $Z_m(K_{m,n}\eta)$ and $\partial/\partial\eta(Z_m(K_{m,n}\eta))$. These eigen values are determined by Equation (11), and are the same both in the radial vortex system and radial source line system since the boundary condition with respect to the radial velocity at the hub and the outer casing wall is the same. However, the eigen values related to the 0-th order Bessel function are required only for the source system. The first three eigen values for each order of Bessel function were found by a step by step procedure and other approximate eigen values were found by extrapolation. Approximate eigen values are improved to obtain higher accuracy by successive interation up to 10^{-9}. The eigen values were obtained for Bessel functions of order m = 0 to 100, and the number of eigen values n = 1 to 20 for each order m for hub-to-tip ratios ν = 0.3 and 0.6 (see Figure 2, 3). The eigen values in Reference (4) are connected with the present $K_{m,n}$ by the following expression:

$$\mu_{m,n} = \nu \cdot K_{m,n} \ .$$

Now, the related functions $F_v(K_{m,n},\nu)$ and $F_s(K_{m,n},\nu)$ are again given by

$$F_v(K_{mn},\nu) = \frac{\int_\nu^1 \eta Z_m(K_{mn}\eta)\,d\eta}{\int_\nu^1 \eta Z_m^2(K_{mn}\eta)\,d\eta} \tag{36}$$

$$F_s(K_{m,n},\nu)=\frac{\int_\nu^1 Q(\eta)\,Z_m(K_{m,n}\eta)\,d\eta}{\int_\nu^1 \eta\cdot Z_m^2(K_{m,n}\eta)\,d\eta}, \quad (37)$$

where Q (η) is the p-th order polynomial given in Equation (38). Then,

$$Q(\eta)=A_0+A_1\cdot\eta+\cdots\cdots\cdots+A_p\cdot\eta^p \quad (38)$$

the numerators of Equations (36) and (37) were resolved into $\int_\nu^1 \eta^p Z_m(K_{m,n}\eta)\,d\eta (p=0 \text{ to } 3)$ and calculated by the Gaussion quadrature formula to order 29 for each eigen value (Reference 5), which is a more accurate numerical integral formula than the trapezoidal or Simpson's formula for the same number of points. The denominators of Equations (36) and (37) were calculated by integral formula for Bessel function for each eigen value. Calculation of $Z_m(K_{m,n}\eta)$ and $\partial/\partial\eta\ (Z_m(K_{m,n}\eta))$ is very time consuming. Therefore, nine radial coordinates are selected from the values calculated by the Gaussian quadrature abscissae and $\eta=\nu$, 1. The radial coordinates for which all related functions and necessary Bessel functions are prepared are given in Tables 1, 2, and 3.

Table 1. Radial Coordinates Used for Computation.

k	1	2	3	4	5	6	7	8	9
η_k	ν	$f(X_7)$	$f(X_{10})$	$f(X_{13})$	$(1+\nu)/2$	$f(X_{17})$	$f(X_{20})$	$f(X_{23})$	1.0

where

$$f(x_i)=((1+\nu)+(1-\nu)\cdot x_i)/2.0 \quad (39)$$

and

$$\begin{aligned} x_7 &= -x_{23} = -0.7524629 \\ x_{10} &= -x_{20} = -0.5075930 \\ x_{13} &= -x_{17} = -0.2113523 \end{aligned} \quad (40)$$

These correspond to the i-th Gaussion abscissa of order 29. The values for $\nu=0.6$ and 0.3 are tabulated in Table 2 and 3 respectively.

Table 2. Radial Coordinates Used for Computation ($\nu=0.6$).

k	1	2	3	4	5	6	7	8	9
η_k	0.60000	0.64951	0.69848	0.75773	0.80000	0.84227	0.90152	0.95049	1.00000

Table 3. Radial Coordinates Used for Computation ($\nu=0.3$).

k	1	2	3	4	5	6	7	8	9
η_k	0.30000	0.38664	0.47234	0.57603	0.65000	0.72397	0.82766	0.91336	1.00000

The values $Z_m(K_{m,n}\eta)$ for the above mentioned radial coordinates are already calculated in the process of evaluating the numerical integral $\int_\nu^1 \eta^p Z_m(K_{m,n}\eta)\,d\eta$ and also the values of $\partial/\partial\eta\ (Z_m(K_{m,n}\eta))$ were calculated by known values using the recurrence formula for the Bessel function. To avoid duplicate calculation of the Bessel function in the main program, all eigen values and related functions were stored on a magnetic tape for $m=0$ to 100, $n=1$ to 20, $\nu=0.3$ and 0.6 for the radial coordinates given in Tables 2 and 3. Then, the computer program for the three-dimensional potential flow field due to an arbitrary series of radial vortex lines of constant strength and a series of radial source lines of variable strength can be used for hub-to-tip ratios $\nu=0.3$ and 0.6 (see Reference 6). Furthermore, if the eigen values and related functions are obtained in a similar manner for any other hub-to-tip ratio, the above computer program is valid for that hub-to-tip ratio as well. The computer programs for the determination of the eigen values and related Bessel functions are given in Reference 6.

4.2 Numerical Calculation of the Three-Dimensional Perturbed Flow Field

4.2.1 Convergency of the Solution of the Three-Dimensional Perturbed Flow Field

The three-dimensional perturbed flow fields due to a series of radial vortex lines of constant strength and a series of radial source lines of variable strength given by Equations (20) to (24) and (31) to (35) include an infinite number of summations with respect to m and n. In order to examine the convergency of the series expressions, a single radial vortex line of strength unity located at $\zeta=0$, $\theta=0°$ and a single radial source line of strength unity located at the same place were examined for $\nu=0.6$ separately. The contributions of m and n to the convergency of the tangential velocity at $\zeta=0.05$, 0.1, 0.2 and $\theta=30°$ for $\eta=0.8$ due to a single radial vortex line are shown in Figure 4. The corresponding graphs for a single radial source line are plotted in Figure 5. It is clear that the convergency of the series expression strongly depends on m, but not on n. For hub-to-tip ratio $\nu=0.6$, the

required order of Bessel function m is approximately $m > 60$ for $|\zeta| < 0.1$, $m > 20$ for $|\zeta| > 0.2$ and $n = 6$ is enough in any case. Therefore, these results suggest that the summation based on only $n = 1$ for each m will give a good result for large $|\zeta|$ if m is taken large enough. However, the convergency becomes poor at points close to the singular point $|\zeta| < 0.05$ for $\nu = 0.6$ even if m is taken up to 100. This situation is more severe in the case of smaller hub-to-tip ratio. It seems the smaller the hub-to-tip ratio is, the more the eigen values are required. The three-dimensional tangential velocity components due to a vortex line and the axial velocity component due to a source line located at $\zeta = 0$ and $\theta = 0°$ must vanish at $\zeta = 0$ for any θ except $\theta = 0°$ for any hub-to-tip ratio from the boundary condition. Therefore, taking advantage of these characteristics of the series expression, some improvement to avoid the above difficulties can be made by further analytical considerations described in Appendix C. This approach will be pursued later.

4.2.2 Three Dimensional Perturbed Flow Field Due to a Single Radial Vortex Line of Strength Unity and Its Comparison with the Two-Dimensional Solution

The three-dimensional perturbed velocity components due to a single radial vortex line of strength unity located at $\zeta = 0$ and $\theta = 0°$ were calculated by Equations (22) to (24) for hub-to-tip ratios $\nu = 0.6$ and 0.3. The corresponding two dimensional values were obtained from Appendix D. The tangential velocity component at the hub due to a single radial vortex line is compared with the two-dimensional values in Figure 6 for $\nu = 0.6$ and Figure 20 for $\nu = 0.3$. The values in the poor convergency region have been excluded. The discrepancy between the three-dimensional and two-dimensional solutions is large for small θ and the maximum difference is about 25% of two-dimensional values for $\nu = 0.6$. The qualitative characteristics of the three-dimensional tangential velocity component are very similar to those of two-dimensional values, and at $\zeta = 0$, $\zeta \to \pm \infty$, the velocities have the same limiting values mathematically (see Appendix C). The effects of the hub-to-tip ratio ν on the tangential velocity component is significant and the maximum difference from the two-dimensional solution is about 30% in the small θ region for $\nu = 0.3$ (see Figure 20). However, accurate three-dimensional values at points close to the singularity could not be obtained due to the poor convergency of the series expression as mentioned in Section 4.2.1.

The tangential velocity components at the mid radius and tip due to a single radial vortex line of strength unity are shown in Figures 7 and 8 for hub-to-tip ratio $\nu = 0.6$, and corresponding graphs for $\nu = 0.3$ are shown in Figures 21 and 22. At mid radius (Figure 7), the discrepancies between the three-dimensional and two-dimensional solutions vanish when the hub-to-tip ratio $\nu = 0.6$, but very small differences were found for $\nu = 0.3$ (see Figure 21). For both $\nu = 0.6$ and 0.3, the three-dimensional tangential velocity components at the hub for small θ are greater than the two-dimensional values, while those at the tip for small θ are smaller than the two-dimensional values (in absolute values). These three-dimensional inviscid effects may partially account for the higher (than the two-dimensional values) lift coefficients measured at the root and lower lift coefficients measured at the tip of a pump rotor by Oshima et al. (Reference 7).

The axial velocity components at the hub, mid radius and tip due to a single radial vortex line of unit strength are shown in Figures 9, 10 and 11 respectively, for hub-to-tip ratio $\nu = 0.6$. Corresponding graphs for $\nu = 0.3$ are shown in Figures 23, 24 and 25 respectively. Similar to the tangential velocity components, the discrepancy between the three-dimensional and two-dimensional axial velocity components vanishes at mid radius for $\nu = 0.6$ (see Figure 10), and very small differences were found at mid radius for $\nu = 0.3$ (see Figure 24). Also, the three-dimensional axial velocity components at the hub for small ζ (< 0.2) are smaller than two-dimensional values (see Figures 9 and 23) for both hub-to-tip ratio $\nu = 0.6$ and 0.3. The magnitude of the discrepancy between the three-dimensional and two-dimensional axial velocity components for small ζ region is 10 to 15% for $\nu = 0.6$. However, for $\nu = 0.3$, for the small ζ region, the numerical results of the three-dimensional axial velocity components are poor. Thus, the discrepancy is not clear, but a larger discrepancy than that for $\nu = 0.6$ may be expected.

The radial velocity components at the mid radius due to a single radial vortex line of strength unity are shown in Figure 12 for $\nu = 0.6$ in Figure 26 for $\nu = 0.3$. The radial velocity components vanish at the hub and the outer casing wall. The typical radial velocity distributions are shown at the mid radius. However, the mid radius is not necessarily the point of maximum radial velocity. The maximum radial velocity usually occurs at a smaller radial coordinate than mid radius. From the comparison of the radial velocity components at mid radius for $\nu = 0.6$ and $\nu = 0.3$, the value for $\nu = 0.3$ is about 3 or 4 times larger than that for $\nu = 0.6$. From analytical considerations, it can be shown that the radial velocity components must vanish at $\zeta = 0$ for all θ except $\theta = 0°$. The graphs do not show the small ζ region due to the lack of convergency of the series expression.

It is clear from the plots shown in Figures 6 to 12 and Figures 20 to 26 that the effects of three-dimensionality are amplified at small hub-to-tip ratio (ν). The order of the magnitude of the radial velocity components is almost 10% of the tangential and axial velocity components for hub-to-tip ratio $\nu = 0.6$, but for $\nu = 0.3$, it is more than 15%. With regard to tangential and axial velocity components, the discrepancy between two-dimensional and three-dimensional solutions is opposite in relative magnitude at the hub and tip locations for any hub-to-tip ratios. This discrepancy increases with decrease in hub-to-tip ratio. Finally, the three-dimensional numerical results were compared with References (2) and (4). The present numerical results for $\nu = 0.6$ are coincident with the results of Reference (4), but different from the results of Reference (2). However, no other numerical results are available for a small hub-to-tip ratio such as $\nu = 0.3$ for comparison.

4.2.3 Three-Dimensional Perturbed Flow Field Due to a Single Radial Source Line of Strength Unity and Its Comparison with the Two-Dimensional Solution

Numerical calculation of the three-dimensional flow field due to a radial source line has not been reported earlier. Even though the flow field around the blades depends mainly on the vortex distribution, the three-dimensional effects due to a source line (representing the thickness) can be of the same order as the three-dimensional effects due to a vortex line. This is especially true when there is appreciable radial variation in blade thickness. The three-dimensional perturbed velocity components due to a single radial source line of strength unity located at $\zeta = 0$ and $\theta = 0°$ were calculated from Equations (33), (34) (35) for the hub-to-tip ratios $\nu = 0.6$ and 0.3. The computer program can be used for the determination of the three-dimensional flow field due to a series of radial source lines of variable strength represented by the third-order polynomials, but only the case of constant strength (= 1.0) is shown in Figures 13 to 19 and Figures 27 to 33 together with two-dimensional solutions.

The tangential velocity components at the hub, mid radius and tip due to a single radial source line of strength unity are shown in Figures 13, 14, and 15 for a hub-to-tip ratio $\nu = 0.6$, and Figures 27, 28, and 29 for $\nu = 0.3$. Consider the two-dimensional flow field due to a vortex of strength unity and a source of strength unity. The magnitude of the two-dimensional tangential velocity components due to a vortex is the same as the two-dimensional axial velocity components due to a source except for the difference of sign. Similarly, the two-dimensional axial velocity components due to a vortex are the same magnitude as the two-dimensional tangential velocity components due to a source. The relative characteristics of the three-dimensional perturbed flow fields due to a single radial vortex line of strength unity and those due to a single radial source line of strength unity are very similar to the relative characteristics of the two-dimensional case as mentioned above. Hence, the three-dimensional tnagential velocity components at the hub due to a single radial source line (see Figure 13) are quite similar to the axial velocity components at the hub due to a single radial vortex line (see Figure 9). However, the discrepancy between two-dimensional and three-dimensional solutions is opposite in relative magnitude. The tangential velocity at the hub due to a source line is larger than the two-dimensional value (see Figure 13), but the axial velocity at the hub due to a vortex line is smaller than the two-dimensional value (see Figure 9). Similarly, the tangential velocity components at the mid radius (see Figure 14) and the tip (see Figure 15) due to a source line are very similar to the axial velocity components at mid radius (see Figure 10) and the tip (see Figure 11) due to a vortex line. It is clear from

Figure 14 that the tangential velocity components at the mid radius due to a source line are the same as the two-dimensional values as in the case of a vortex (see Figure 10). The tangential velocity components at the tip due to a source line shown in Figure 15 are smaller than the two-dimensional values; however, in the corresponding graph of Figure 11, the axial velocity due to a vortex line is larger than that of the two-dimensional value. Comparing the tangential velocity components at the hub and at the tip due to a source line we find that at the hub the three-dimensional values are larger than the corresponding two-dimensional values while at the tip they are smaller than the two-dimensional values. The above discussion for the three-dimensional tangential velocity components due to a source line for the hub-to-tip ratio $\nu = 0.6$ is qualitatively valid for the case of the hub-to-tip ratio $\nu = 0.3$. Specifically, Figures 27, 28, and 29 are similar to Figures 23, 24, and 25 respectively, and the characteristics of the three-dimensional tangential velocity components relative to the two-dimensional values for $\nu = 0.3$ due to a source line are the same as those for hub-to-tip ratio $\nu = 0.6$. The relative behavior of the tangential velocity for $\nu = 0.3$ due to a source line at the hub and tip is also quite similar to that for $\nu = 0.6$. However, the magnitude of the discrepancy between the three-dimensional tangential velocity components due to a source line and those for the two-dimensional case is amplified by small hub-to-tip ratio (ν). At mid radius, the tangential velocity components for $\nu = 0.3$ due to a source line are slightly different from the two-dimensional values.

The axial velocity components at the hub, mid radius and tip due to a single radial source line of strength unity are shown in Figures 16, 17, and 18 for hub-to-tip ratio $\nu = 0.6$, and in Figures 30, 31, and 32 for $\nu = 0.3$ respectively. The axial velocity at the hub due to a source line for $\nu = 0.6$ shown in Figure 16 is similar to the tangential velocity at the hub due to a vortex line except for the difference of sign. In the same way, Figures 17 and 18 are similar to Figures 7 and 8 respectively. The axial velocity at mid radius due to a source line shown in Figure 17 is the same as the tangential velocity due to a vortex line, and the discrepancies between the three-dimensional and two-dimensional values vanish. The relative behavior of the axial velocity due to a source line at the hub and tip is such that, in the small ζ region, the three-dimensional axial velocity components at the hub are smaller than those for the two-dimensional case, but at the tip the three-dimensional values are larger than the two-dimensional values (see Figures 16 and 18). For the case of the small hub-to-tip ratio $\nu = 0.3$, the earlier comments are still valid, but the discrepancies between the three-dimensional axial velocity components due to a source line and the corresponding two-dimensional values are amplified by the small hub-to-tip ratio (see Figures 30, 31, and 32). Then, the axial velocity at the mid radius for $\nu = 0.3$ due to a source line is slightly different from the two-dimensional axial velocity component. This may be partly due to poor convergency of series expressions, but the remaining part of the discrepancies may be due to essential characteristics of small hub-to-tip ratio since mid radius is not necessarily the point of the same velocity as predicted by the two-dimensional theory. The closed form of the tangential and radial velocity component due to a single radial source line of strength unity is not known so far, but the axial velocity component due to a source line vanishes at $\zeta = 0$ for any θ except $\theta = 0°$, similar to the two-dimensional analysis. However, the limiting value at $\zeta \to \pm\infty$, is different from the two-dimensional solution since at $\zeta \to \pm\infty$, $(u_{s\zeta})_{3d} = \pm 1/(2\pi(1+\nu))$ in the three-dimensional case and $(u_{s\zeta})_{2d} = \pm 1/(4\pi\eta)$ in two-dimensional flow. Therefore, these limiting values are identical only for the mid radius($\eta = (1+\nu)/2$), as shown in Figures 30, 31, and 32.

The radial velocity components at the typical radial coordinate $\eta = (1+\nu)/2$ due to a single radial source line of strength unity are shown in Figure 19 for $\nu = 0.6$ and in Figure 33 for $\nu = 0.3$, respectively. The behavior of the radial velocity components due to a source line are completely different from those due to a vortex line.

5. CONCLUSION

The investigation reported in this paper indicates that the three dimensional effects due to finite radius hub and annulus walls on the flow filed induced by a radial vortex or a source line spanning an annulus is appreciable, and these three-dimensional effects increase with decrease in hub/tip ratio. The discrepancy between the three and two dimensional solutions,

which may be as high as 50% for the cases investigated here, is dominant near the hub due to small radius of curvature. The discrepacy between the two solutions is negligibly small at the mid radius, and are in opposite directions at the hub and tip.

ACKNOWLEDGEMENTS

The author wishes to express sincere appreciation to his advisor, Dr. B. Lakshminarayana, for his help and counsel during the investigation. The work was sponsored by the applied research Laboratory of The Pennsylvania State University which operates under contract with the Naval Ordnance System Command. Dr. M. T. Pigott is to be credited for encouraging such a basic research which is so vital in understanding the complex phenomena in turbomachinery.

REFERENCES

[1] Meyer, R. "Beitrag zur Theories feststehender Schaufelgitter," Mitt. Aus Dem Inst. Aerodynamic (E.T.H., Zurich) Report 11, 1946 (Publisher, Verlag Leeman, Zurich. English Translation ARC 8869).

[2] Tyson, R. N., Jr. "Three-Dimensional Interference Effects of a Finite Number of Blades in an Axial Turbomachine," November 1952, California Institute of Technology, Hydrodynamics Laboratory, Report No.E-19.1.

[3] Rossow, Vernon J. "An Analysis of the Error Involved in Unrolling the Flow Field in Turbine Problem," Mitt Aus Dem Inst. Aerodynamik (E.T.H., Zurich) Report 23, 1957 (Publisher, Verlag Leeman, Zurich).

[4] Etter, R. J. and van Dyke, P., "Three-Dimensional Flow Field from a Radial Vortex Filament," December 1969, Hydronautics Incorporated Technical Report 703-7.

[5] Love, Carl H. "Abscissas and Weights for Gaussian Quadrature for N = 2 to 100, and N = 125, 150, 175, 200," December 1966, National Bureau of Standard Monograph 98.

[6] Tamura, A., Howells, R., and Lakshminarayana, B. "Three-Dimensional Potential Flow Around a Body Spanning an Annulus: Computer Program and Solution," Applied Research Laboratory, The Pennsylvania State University. Technical Memorandum 73–173, 1973.

[7] Oshima, M., et al. "Blade Characteristics of Axial Impellers," Proc. 2nd Int. JSME Symposium on Fluid Machinery and Fluidics, Tokyo, Japan, Vol. 1, 1973, p. 119.

[8] Watson, G. N. *Theory of Bessel Functions.* Cambridge University Press, 1958.

[9] Milne-Thomson, L. M. *Theoretical hydrodynamics.* McMillan, 1968.

APPENDIX A

Specification of the Boundary Condition for Radial Vortex Line and Source Line

Specification of the Boundary Conditions for a Radial Vortex Line

The single radial vortex line of constant strength Γ located at $\zeta = 0$, $\theta = 0°$ is split into $\gamma d\omega$ (see Figure a) and distributed over $-\delta/2 < 0 < \delta/2$ as given by

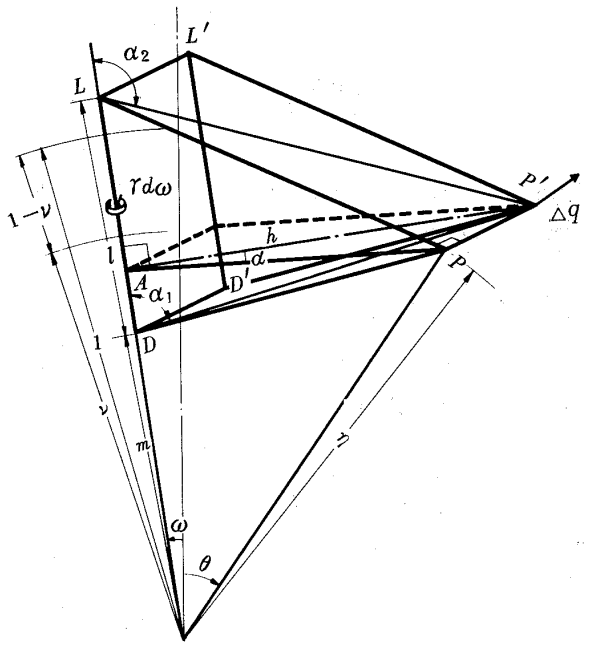

Fig. a Split Radial Vortex Line

$$\int_{-\delta/2}^{\delta/2} \gamma d\omega = \gamma\delta = \Gamma \tag{A1}$$

The induced velocity $\triangle q$ at $(\eta, \theta, \delta/2)$ due to $\gamma d\omega$ is given by

$$\triangle q = \gamma d\omega / 4\pi h (\cos \alpha_1 - \cos \alpha_2), \tag{A2}$$

where

$$\cos \alpha_1 = \frac{\overline{AD}}{\overline{DP'}} = \frac{\eta \cos (\theta - \omega) - m}{\sqrt{\eta^2 + m^2 + (\triangle\zeta/2)^2 - 2m\eta \cos (\theta - \omega)}}, \tag{A3}$$

$$\cos \alpha_2 = \frac{\overline{AL}}{\overline{P'L}} = \frac{\ell + m - \eta \cos (\theta - \omega)}{\sqrt{\eta^2 + (\ell + m)^2 + (\triangle\zeta/2)^2 - 2 (\ell + m) \eta \cos (\theta - \omega)}} \tag{A4}$$

and

$$\sin \alpha = \frac{\overline{PP'}}{h} = \frac{\triangle\zeta/2}{\sqrt{\eta^2 \sin^2 (\theta - \omega) + (\triangle\zeta/2)^2}}. \tag{A5}$$

Therefore, the tangential velocity component of the induced velocity due to the total of the split radial vortex lines is given by

$$\begin{aligned} v_\theta &= \int_{-\delta/2}^{\delta/2} \triangle q \sin \alpha \cos (\theta - \omega) d\omega \\ &= \frac{\gamma}{4\pi} \int_{-\delta/2}^{\delta/2} \frac{\triangle\zeta/2 \cos (\theta - \omega)}{\eta^2 \sin^2 (\theta - \omega) + (\triangle\zeta/2)^2} \\ &\quad \left\{ \frac{\eta \cos (\theta - \omega) - m}{\sqrt{\eta^2 + m^2 + (\triangle\zeta/2)^2 - 2m\eta \cos (\theta - \omega)}} + \right. \\ &\quad \left. \frac{\ell + m - \eta \cos (\theta - \omega)}{\sqrt{\eta^2 + (\ell + m)^2 + (\triangle\zeta/2)^2 - 2 (\ell + m)}} \right\} d\omega \end{aligned} \tag{A6}$$

Integrate with respect to ω and take the limit as $\triangle\zeta \to 0$; then,

$$\lim_{\triangle\zeta \to 0} v_\theta = \gamma/2\eta, \quad \text{for} \quad -\delta/2 < \theta < \delta/2. \tag{A7}$$

Specification of the Boundary Conditions for a Radial Source Line

In the same way as for the vortex line, a radial source line of variable strength $Q(\eta)$ located at $\zeta = 0$, $\theta = 0°$ is split into $\mu(\eta) d\omega$ (see Figure b) and distributed over $-\delta/2 < 0 < \delta/2$ as given by

$$\int_{-\delta/2}^{\delta/2} \mu(\eta)\, d\omega = \mu(\eta)\delta = Q(\eta) \tag{A8}$$

The induced velocity due to a split source $\mu(\eta)$ is represented by

$$\triangle q = \frac{\mu(\eta)\, d\omega}{2\pi \sqrt{\eta^2 \sin^2 (\theta - \omega) + (\triangle\zeta/2)^2}} \tag{A9}$$

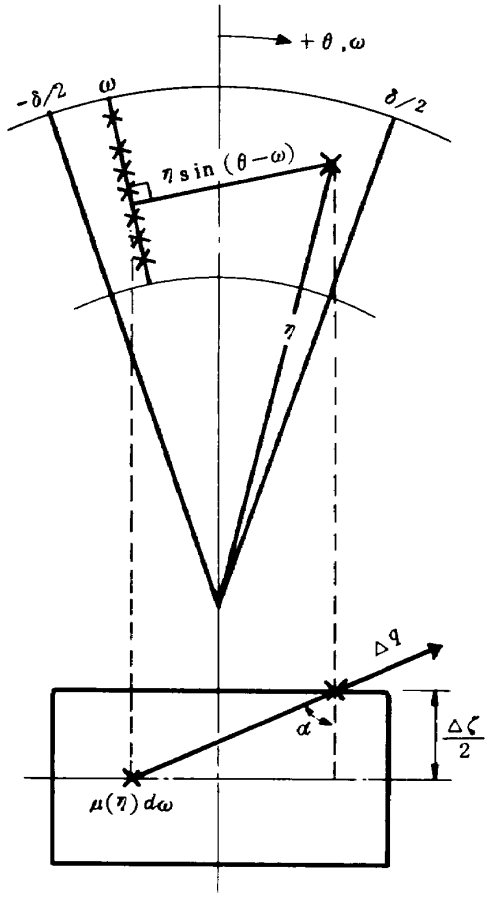

Fig. b Split Radial Source Line

The axial component of the induced velocity due to the total of the split radial source lines is given by

$$v_\zeta = \int_{-\delta/2}^{\delta/2} \Delta q \cos\alpha \, d\omega$$

$$= \frac{\Delta\zeta}{4\pi} \int_{-\delta/2}^{\delta/2} \frac{\mu(\eta)}{\eta \sin^2(\theta-\omega) + (\Delta\zeta/2)^2} \, d\omega \, . \tag{A10}$$

Integrate and take a limit as $\Delta\zeta \to 0$; then,

$$\lim_{\Delta\zeta \to 0} v_\zeta = \mu(\eta)/2\eta \, , \quad \text{for } -\delta/2 < \theta < \delta/2 \, . \tag{A11}$$

APPENDIX B

Related Bessel Function and Characteristics of the Series Expression

a) Function $Z_m(K_{mn}\eta)$

$$Z_m(K_{mn}\eta) = J_m(K_{mn}\eta) \left[\frac{\partial Y_m(K_{mn}\eta)}{\partial\eta}\right]_{\eta=1} - \left[\frac{\partial J_m(K_{mn}\eta)}{\partial\eta}\right]_{\eta=1} Y_m(K_{mn}\eta) \, . \tag{A12}$$

From Equation (A12)

$$Z_m(K_{mn}\eta) = K_{mn}\left\{ J_m(\chi) \cdot \left[\frac{\partial Y_m(\chi)}{\partial\chi}\right]_{\chi=K_{mn}} - \left[\frac{\partial J_m(\chi)}{\partial\chi}\right]_{\chi=K_{mn}} \cdot Y_m(\chi) \right\} ,$$

where $\chi = K_{mn}\eta$. Then by Lommel's formula for Bessel Function,

$$\left[Z_m(K_{mn}\eta)\right]_{\eta=1} = K_{mn}\left[\frac{2}{\pi\chi}\right] = \frac{2}{\pi} \tag{A13}$$

and also from the boundary condition given by Equation (11) in Section 3.1,

$$\frac{J_m'(K_{mn}\nu)}{Y_m'(K_{mn}\nu)} = \frac{J_m'(K_{mn})}{Y_m'(K_{mn})} \tag{A14}$$

Then,

$$Z_m(K_{mn}\eta) = \frac{Y_m'(K_{mn})}{Y_m'(K_{mn}\nu)} \bar{Z}_m(K_{mn}\eta) \, , \tag{A15}$$

where

$$\bar{Z}_m(K_{mn}\eta) = J_m(K_{mn}\eta) Y_m'(K_{mn}\nu) - J_m'(K_{mn}\nu) Y_m(K_{mn}\eta) \, .$$

Therefore

$$\left[\bar{Z}_m(K_{mn}\eta)\right]_{\eta=\nu} = \left[\bar{Z}_m(\chi)\right]_{\chi=K_{mn}\nu}$$

$$= K_{mn}\left[J_m(\chi) \frac{\partial Y_m(\chi)}{\partial\chi} - \frac{\partial J_m(\chi)}{\partial\chi} Y_m(\chi)\right]_{\chi=\nu K_{mn}}$$

by Lommel's formula

$$\left[\bar{Z}_m(K_{mn}\eta)\right]_{\eta=\nu} = K_{mn}\left[\frac{2}{\pi\chi}\right]_{\chi=K_{mn}\nu} = \frac{2}{(\nu\pi)} \, .$$

Hence,

$$\left[Z_m(K_{mn}\eta)\right]_{\eta=\nu} = \frac{2}{\nu\pi} \frac{Y_m'(K_{mn})}{Y_m'(K_{mn}\nu)} \, . \tag{A16}$$

b) Integral and Derivatives of $Z_m(K_{mn}\eta)$

From boundary condition (A14),

$$\left[\frac{\partial Z_m(K_{mn}\eta)}{\partial \eta}\right]_{\eta=1,\nu} = 0 \tag{A17}$$

$$\frac{\partial^2 Z_m(K_{mn}\eta)}{\partial \eta^2} = \begin{cases} \frac{2}{\pi}(m^2 - K_{mn}^2) & \text{when } \eta = 1 \\ \frac{2}{\nu\pi}\left(\frac{m^2}{\nu^2} - K_{mn}^2\right)\frac{Y_m'(K_{mn})}{Y_m'(K_{mn}\nu)} & \text{when } \eta = \nu \end{cases} \tag{A18}$$

and

$$\int_\nu^1 \eta Z_m^2(K_{mn}\eta)\, d\eta = \frac{1}{K_{mn}^2}\int_{K_{mn}\nu}^{K_{mn}} S Z_m^2(S)\, dS = \frac{1}{K_{mn}^2}\left[\frac{S^2}{2}\left(\left(1-\frac{m^2}{S^2}\right)Z_m^2(S) + Z_m'^2(S)\right)\right]_{K_{mn}\nu}^{K_{mn}}, \tag{A19}$$

where $\left[Z_m'(S)\right]_{S=K_{mn},K_{mn}\nu} = 0$.

c) Closed Form for Series Expression

By Dini's expansion,

$$\sum_{n=1}^{\infty}\frac{\int_\nu^1 \eta Z_m(K_{mn}\eta)\, d\eta}{\int_\nu^1 \eta Z_m^2(K_{mn}\eta)\, d\eta} Z_m(K_{mn}\eta) = 1, \tag{A20}$$

using Equation (A13), we obtain

$$\sum_{n=1}^{\infty}\frac{\int_\nu^1 \eta Z_m(K_{mn}\eta)\, d\eta}{\int_\nu^1 \eta Z_m^2(K_{mn}\eta)\, d\eta} = \frac{\pi}{2} . \tag{A21}$$

The tangential and radial velocity components due to a single radial vortex line and also the axial velocity component due to a single radial source line are zero at $\zeta = 0$.

$$(u_{v\theta})_{\zeta=0} = \mp\frac{\Gamma}{4\pi\eta}\left(1 + 2\sum_{m=1}^{\infty}\cos m\theta \cdot \sum_{n=1}^{\infty}\frac{\int_\nu^1 \eta Z_m(K_{mn}\eta)\, d\eta}{\int_\nu^1 \eta Z_m^2(K_{mn}\eta)\, d\eta} Z_m(K_{mn}\eta)\right) = 0, \tag{A22}$$

$$(u_{v\eta})_{\zeta=0} = \mp\frac{\Gamma}{2\pi}\sum_{m=1}^{\infty}\frac{\sin m\theta}{m} \cdot \sum_{n=1}^{\infty}\frac{\int_\nu^1 \eta Z_m(K_{mn}\eta)\, d\eta}{\int_\nu^1 \eta Z_m^2(K_{mn}\eta)\, d\eta}\frac{\partial Z_m(K_{mn}\eta)}{\partial \eta} = 0 \tag{A23}$$

and

$$(u_{s\zeta})_{\zeta=0} = \frac{1}{4\pi}\left(\pm\frac{2}{1-\nu^2}\int_\nu^1 Q(\eta)\, d\eta \pm \sum_{n=2}^{\infty}\frac{\int_\nu^1 Q(\eta) Z_o(K_{on}\eta)\, d\eta}{\int_\nu^1 \eta Z_o^2(K_{on}\eta)\, d\eta} Z_o(K_{on}\eta) \pm 2\sum_{m=1}^{\infty}\cos m\theta \sum_{n=1}^{\infty}\frac{\int_\nu^1 Q(\eta) Z_m(K_{mn}\eta)\, d\eta}{\int_\nu^1 \eta Z_m^2(K_{mn}\eta)\, d\eta} \cdot Z_m(K_{mn}\eta) = 0\right) \tag{A24}$$

The tangential and radial velocity components due to a single radial vortex line of constant strength should have an inflection point at $\zeta = 0$; then,

$$\left[\frac{\partial^2 u_{v\theta}}{\partial \zeta^2}\right]_{\zeta=0} = \mp\frac{\Gamma}{2\pi\eta}\sum_{m=1}^{\infty}\cos m\theta \cdot \sum_{n=1}^{\infty} K_{mn}^2\frac{\int_\nu^1 \eta Z_m(K_{mn}\eta)\, d\eta}{\int_\nu^1 \eta Z_m^2(K_{mn}\eta)\, d\eta} Z_m(K_{mn}\eta) = 0 \tag{A25}$$

and

$$\left[\frac{\partial^2 u_{v\eta}}{\partial \zeta^2}\right]_{\zeta=0} = \mp\frac{\Gamma}{2\pi}\sum_{m=1}^{\infty}\frac{\sin m\theta}{m} \cdot \sum_{n=1}^{\infty} K_{mn}^2\frac{\int_\nu^1 \eta Z_m(K_{mn}\eta)\, d\eta}{\int_\nu^1 \eta Z_m^2(K_{mn}\eta)\, d\eta} \cdot \frac{\partial Z_m(K_{mn}\eta)}{\partial \eta} = 0 . \tag{A26}$$

Also, the axial velocity component due to a single radial vortex line of constant strength has a maximum value at $\zeta = 0$; then,

$$\left(\frac{\partial u_{v\zeta}}{\partial \zeta}\right)_{\zeta=0} = \mp \frac{\Gamma}{2\pi} \sum_{m=1}^{\infty} \frac{\sin m\theta}{m} \cdot$$

$$\sum_{n=1}^{\infty} K_{mn}^2 \frac{\int_{\nu}^{1} \eta Z_m(K_{mn}\eta)\, d\eta}{\int_{\nu}^{1} \eta Z_m^2(K_{mn}\eta)\, d\eta} \cdot Z_m(K_{mn}) = 0 \ . \tag{A27}$$

Similarly, for the three-dimensional flow field due to a single radial source line of variable strength, the tangential and radial velocity components have a maximum value at $\zeta = 0$; then,

$$\left(\frac{\partial u_{s\theta}}{\partial \zeta}\right)_{\zeta=0} = \mp \frac{\Gamma}{2\pi\eta} \sum_{m=1}^{\infty} m \sin m\theta \cdot$$

$$\sum_{n=1}^{\infty} \frac{\int_{\nu}^{1} Q(\eta) Z_m(K_{mn}\eta)\, d\eta}{\int_{\nu}^{1} \eta Z_m^2(K_{mn}\eta)\, d\eta} \cdot Z_m(K_{mn}\eta)\, d\eta = 0 \tag{A28}$$

and

$$\left(\frac{\partial u_{s\eta}}{\partial \zeta}\right)_{\zeta=0} = -\frac{1}{4\pi}\left(\mp \sum_{n=2}^{\infty} \frac{\int_{\nu}^{1} Q(\eta) Z_o(K_{on}\eta)\, d\eta}{\int_{\nu}^{1} \eta Z_o^2(K_{on}\eta)\, d\eta} \cdot \right.$$

$$\frac{\partial Z_o(K_{on}\eta)}{\partial \eta} \pm 2 \sum_{m=1}^{\infty} \cos m\theta \cdot$$

$$\left. \sum_{n=1}^{\infty} \frac{\int_{\nu}^{1} Q(\eta) Z_m(K_{mn}\eta)\, d\eta}{\int_{\nu}^{1} \eta Z_m^2(K_{mn}\eta)\, d\eta} \frac{\partial Z_m(K_{mn}\eta)}{\partial \eta} \right) = 0 \ . \tag{A29}$$

The axial velocity component has an inflection point at $\zeta = 0$; then,

$$\left(\frac{\partial^2 u_{s\zeta}}{\partial \zeta^2}\right)_{\zeta=0} = \frac{1}{4\pi}\left(\mp \sum_{n=2}^{\infty} K_{on} \frac{\int_{\nu}^{1} Q(\eta) Z_o(K_{on}\eta)\, d\eta}{\int_{\nu}^{1} \eta Z_o^2(K_{on}\eta)\, d\eta} \cdot \right.$$

$$Z_o(K_{on}\eta) \mp 2 \sum_{m=1}^{\infty} \cos m\theta \sum_{n=1}^{\infty} K_{mn} \cdot$$

$$\left. \frac{\int_{\nu}^{1} Q(\eta) Z_m(K_{mn}\eta)\, d\eta}{\int_{\nu}^{1} \eta Z_m^2(K_{mn}\eta)\, d\eta} Z_m(K_{mn}\eta) \right) = 0 \ . \tag{A30}$$

APPENDIX C

Approximate Formula for the Solution of the Three-Dimensional Flow Field

The solutions of the three-dimensional flow field due to a single radial vortex line and source line include series summations of Bessel functions and trigonometric functions and are quite complicated. A modification of the three-dimensional solutions will be attempted here. The qualitative behavior of the three-dimensional flow filed is similar to the two-dimensional unrolled solution. The perturbed velocities are approximately identical for both two-dimensional and three-dimensional cases at mid radius for any hub-to-tip ratio. Rossow (3) suggested the use of Taylor expansion for the exact solution of the three-dimensional flow field due to a single radial vortex line as an approximate formula may not be balid for small hub-to-tip ratios because of the assumption made in the process of the Taylor expansion. In the process of calculating the three-dimensional flow field, duplicate calculations are required in order to superimpose the effects of the vortex and source lines. Once the basic solutions are obtained, the superposition of the flow field for several vortex and source lines involves only simple algebraic equations. Therefore, if the basic solutions are represented by simple approximate formula based on numerical results of the basic solutions, these approximate formula are valid for any calculation for the same hub-to-tip ratio. Several approximate formulations are suggested below:

a) Approximate velocity potential and velocity components due to a single radial vortex line of constant strength

$$(\Phi_v)_{ap} = -\frac{\Gamma}{2\pi} \tan^{-1} \frac{\tan(\theta/2)}{\tanh(B\zeta)} \tag{A31}$$

$$(u_{v\theta})_{ap} = -\frac{\Gamma}{4\pi\eta} \frac{\sinh(2B\zeta)}{\cosh(2B\zeta) - \cos\theta} \tag{A32}$$

$$(u_{v\eta})_{ap} = -\frac{\Gamma}{2\pi} \frac{B'\zeta \sin\theta}{\cosh(2B\zeta) - \cos\theta} \tag{A33}$$

and

$$(u_{v\zeta})_{ap} = \frac{\Gamma}{2\pi} \frac{B \sin\theta}{\cosh(2B\zeta) - \cos\theta} \ , \tag{A34}$$

where $B = B(\eta)$, $B' = \partial B(\eta)/\partial\eta$. These are similar to the two-dimensional unrolled solutions except for the radial velocity (see Appendix D). The functional behavior of the approximate formula are found to be quite similar to the three-dimensional exact solutions. The approximate tangential and radial velocity components have the same limiting values at $\zeta \to \pm 0$ and $\zeta \to \pm\infty$ as the three-dimensional exact solutions. Also, the approximate tangential and radial velocity components have inflection points at $\zeta = 0$ and the axial velocity component has a maximum at $\zeta = 0$. However, the functions $B(\eta)$ and $B'(\eta)$ are unknown. But, from numerical results of the exact solution at the particular η and θ, the values $B(\eta)$ and $B'(\eta)$ in Equations (A32), (A33) and (A34) can be determined. The development of these approximate solutions is planned for the future.

b) Approximate velocity potential and velocity components due to a single radial source line of constant strength:

The approximate formula for the three-dimensional flow field due to a single radial source line of variable strength can be written as

$$(\Phi_s)_{ap} = \frac{Q}{4\pi(1+\nu)C}\ell n\left(2(\cosh(2C\zeta)-\cos\theta)\right), \tag{A35}$$

$$(u_{s\theta})_{ap} = \frac{Q}{4\pi(1+\nu)C\eta}\frac{\sin\theta}{\cosh(2C\zeta)-\cos\theta}, \tag{A36}$$

$$(u_{s\eta})_{ap} = -\frac{QC'}{4\pi(1+\nu)C}\left(1+\frac{1}{C}\right)\ell n(2(\cosh(2C\zeta)-\cos\theta)) - \frac{2\zeta\sinh(2C\zeta)}{\cosh(2C\zeta)-\cos\theta} \tag{A37}$$

and

$$(u_{s\zeta})_{ap} = \frac{Q}{2\pi(1+\nu)}\frac{\sin(2C\zeta)}{\cosh(2C\zeta)-\cos\theta}, \tag{A38}$$

where $C = C(\eta)$, $C' = \partial C(\eta)/\partial\eta$, and $C = 1/(2\eta)$ correspond to the two-dimensional unrolled solutions (see Appendix D). Again, the functions $C(\eta)$ and $C'(\eta)$ are unknown, similar to the vortex system. These quantities will be determined for fixed η and θ. The values $C(\eta)$ and $C'(\eta)$ so derived are valid for the estimation of the velocity components along the ζ axis for particular η, θ. Values of B, B', C and C' of the present formula, whose functional behavior are quite similar to the corresponding exact solutions, will be determined by using the exact numerical results at a few points for particular η, θ and ζ. Then, the approximate velocity components at any ζ coordinate can be easily determined.

APPENDIX D

Two-Dimensional Unrolled Solution

The velocity potential due to a vortex of strength Γ and a source of strength Q located at $\zeta = 0$ and $\theta = 0$ are given by

$$\Phi_v = -\frac{\Gamma}{2\pi}\tan^{-1}\frac{\tan(\theta/2)}{\tanh(\zeta/(2\eta))} \tag{A39}$$

and

$$\Phi_s = \frac{Q}{4\pi}\ell n\left(2(\cosh(\zeta/\eta)-\cos\theta)\right). \tag{A40}$$

The corresponding velocity components are:

$$u_{v\theta} = -\frac{\Gamma}{4\pi\eta}\frac{\sinh(\zeta/\eta)}{\cosh(\zeta/\eta)-\cos\theta}, \tag{A41}$$

$$u_{v\zeta} = \frac{\Gamma}{4\pi\eta}\frac{\sin\theta}{\cosh(\zeta/\eta)-\cos\theta}, \tag{A42}$$

$$u_{s\theta} = \frac{Q}{4\pi\eta}\frac{\sin\theta}{\cosh(\zeta/\eta)-\cos\theta} \tag{A43}$$

and

$$u_{s\zeta} = \frac{Q}{4\pi\eta}\frac{\sinh(\zeta/\eta)}{\cosh(\zeta/\eta)-\cos\theta}, \tag{A44}$$

where the positive direction of Γ is based on the right-hand screw rule, and the positive and negative values of Q correspond to a source and sink, respectively.

LIST OF FIGURES

LIST OF FIGURES (tinued)

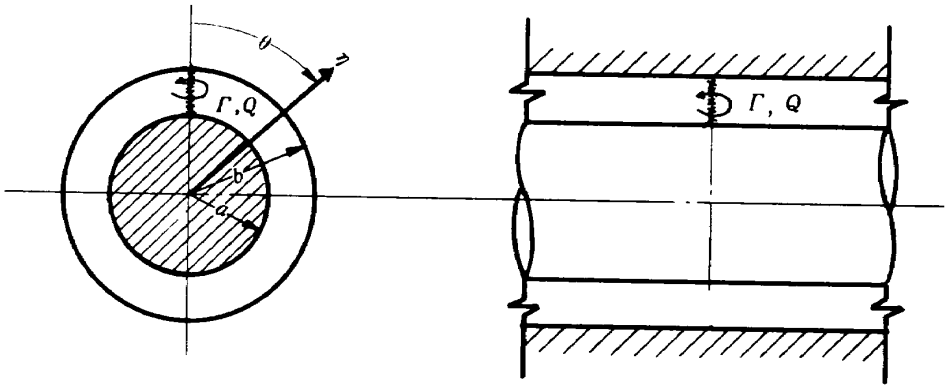

Fig. 1 Single Radial Vortex and Source Line

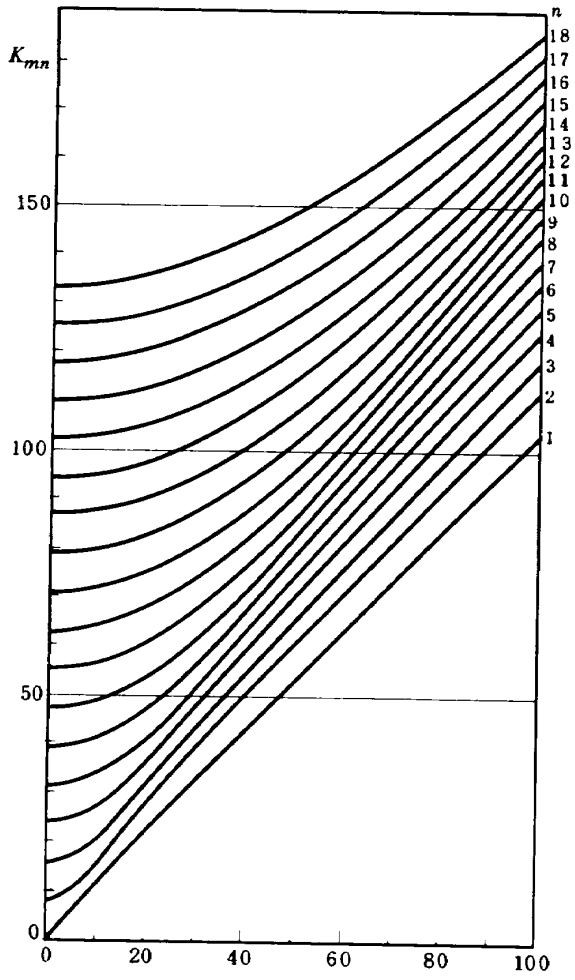

Fig. 2 Eigen Values for ν = 0.6

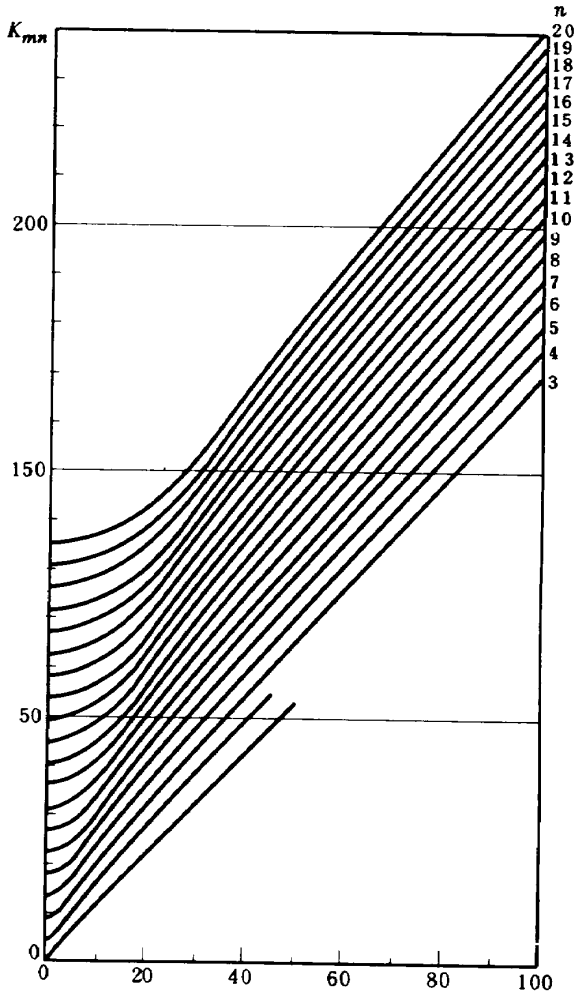

Fig. 3 Eigen Values for ν = 0.3

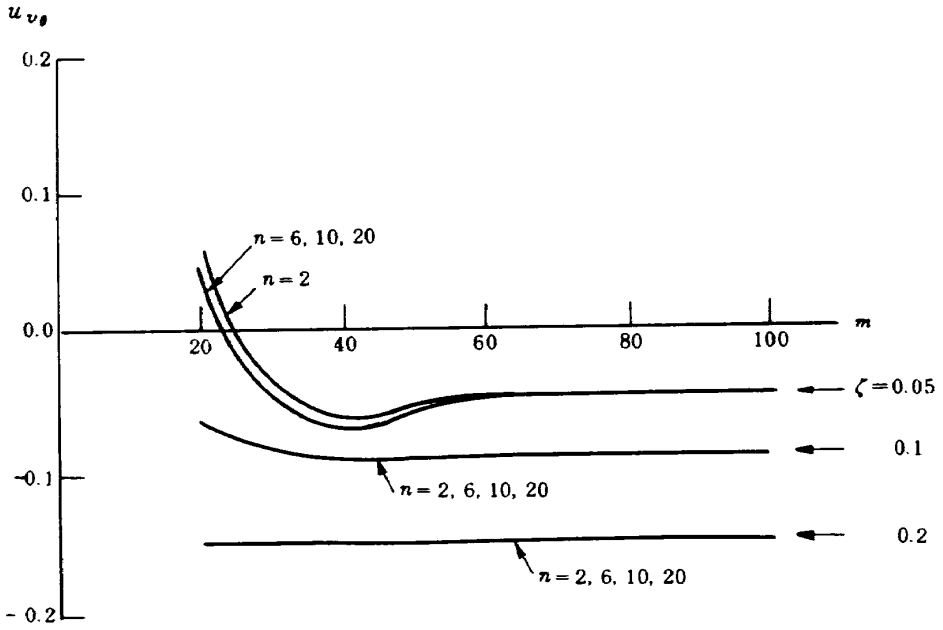

Fig. 4 Convergency of $u_{v\theta}$ = 30°, η = 0.8 for ν = 0.6

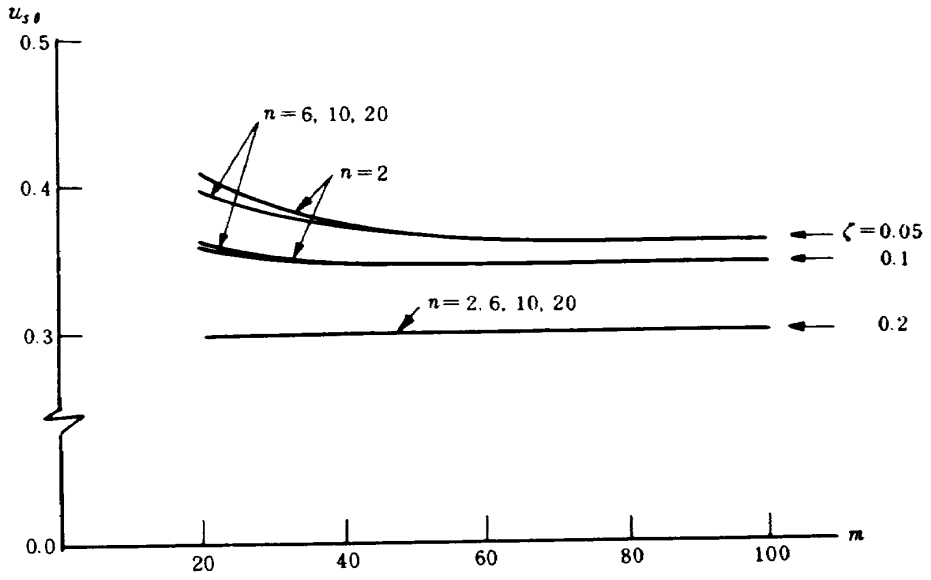

Fig. 5 Convergency of $u_{s\theta}$ at θ = 30°, η = 0.8 for ν = 0.6

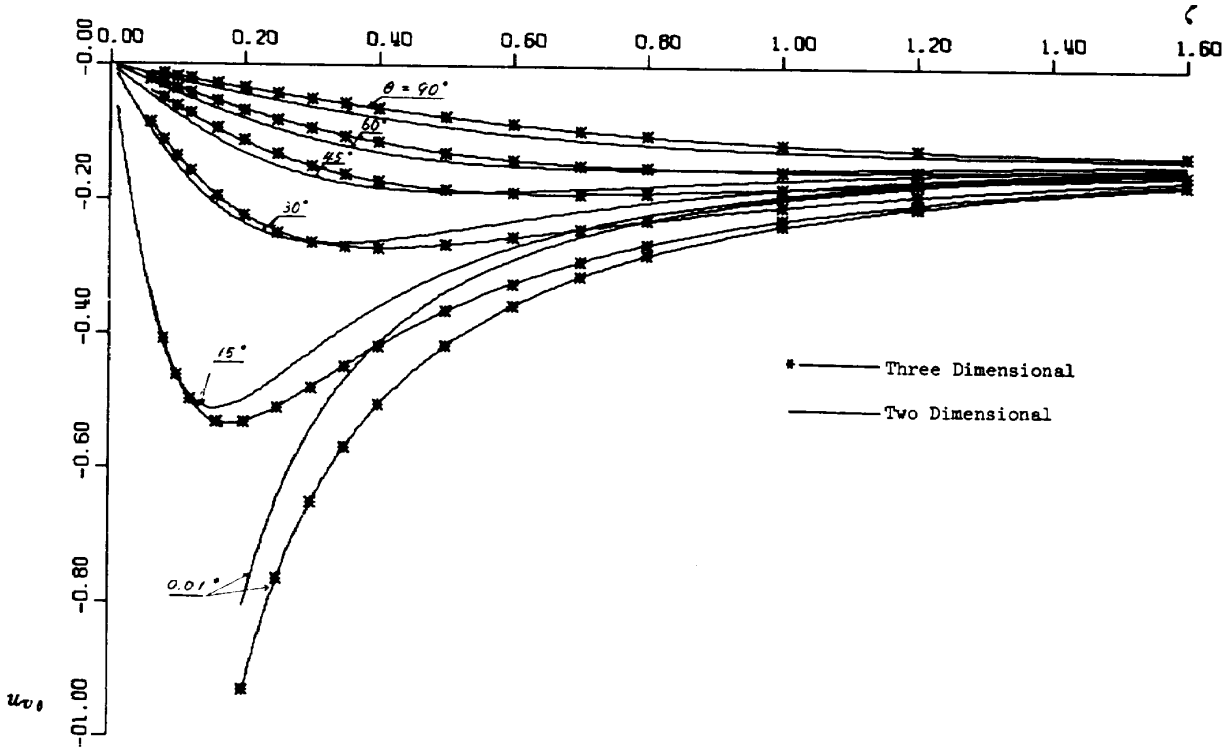

Fig. 6 Tangential Velocity Distribution $u_{v\theta}$ at the Hub(η = 0.6) due to a Single Radial Vortex Line of Strength Unity for ν = 0.6

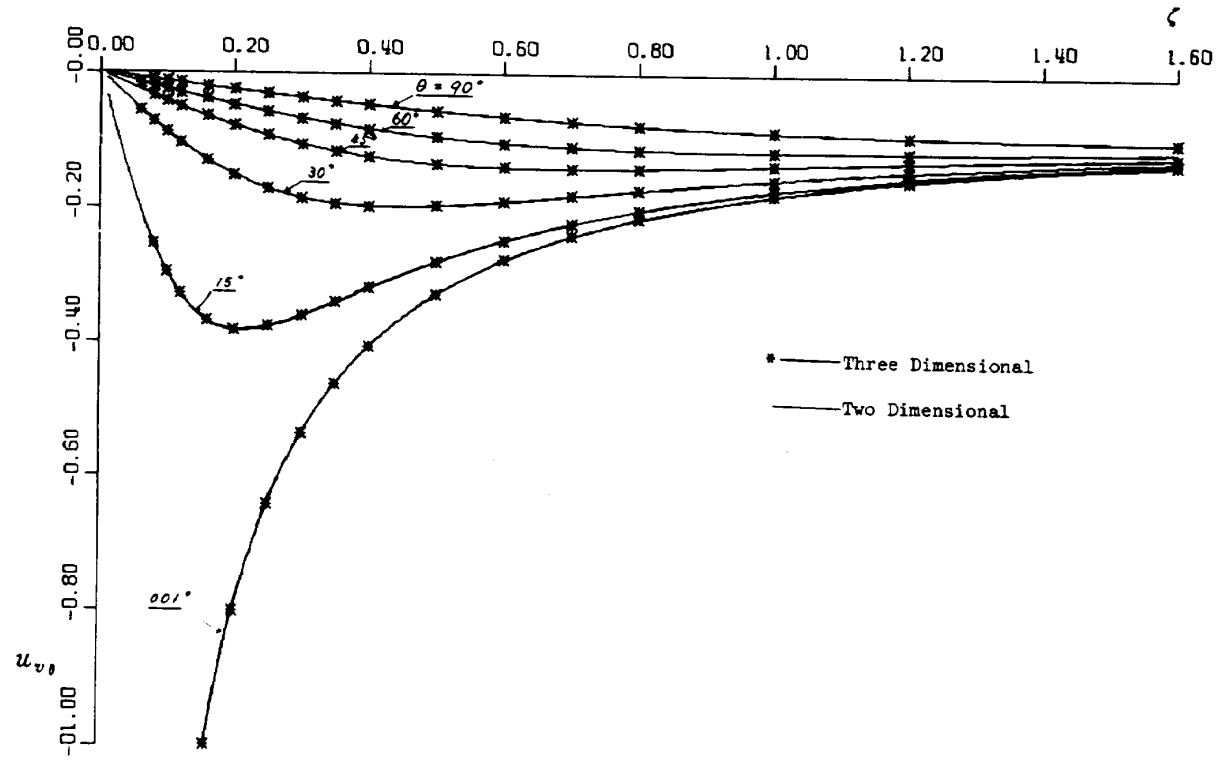

Fig. 7 Tangential Velocity Distribution $u_{v\theta}$ at the Mid Radius(η = 0.8) due to a Single Radial Vortex Line of Strength Unity for ν = 0.6

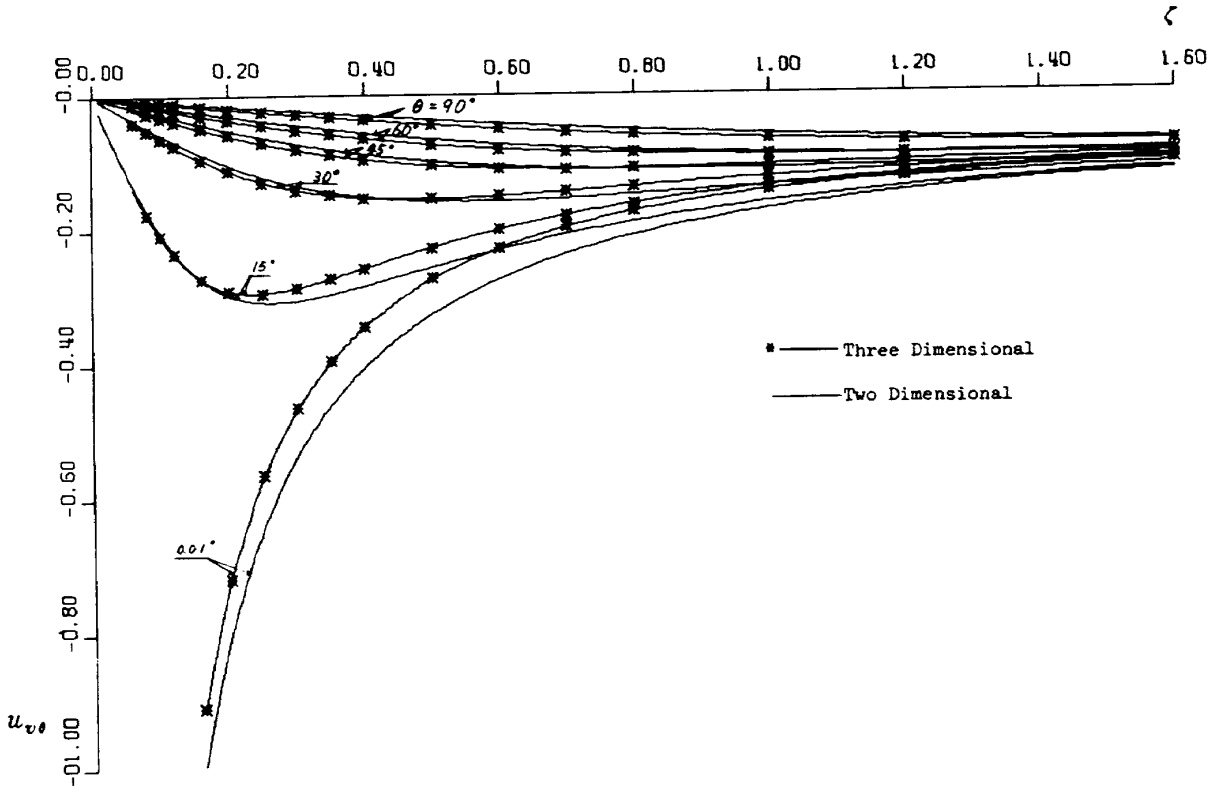

Fig. 8 Tangential Velocity Distribution $u_{v\theta}$ at the Tip (η = 1.0) due to a Single Radial Vortex line of Strength Unity for ν = 0.6

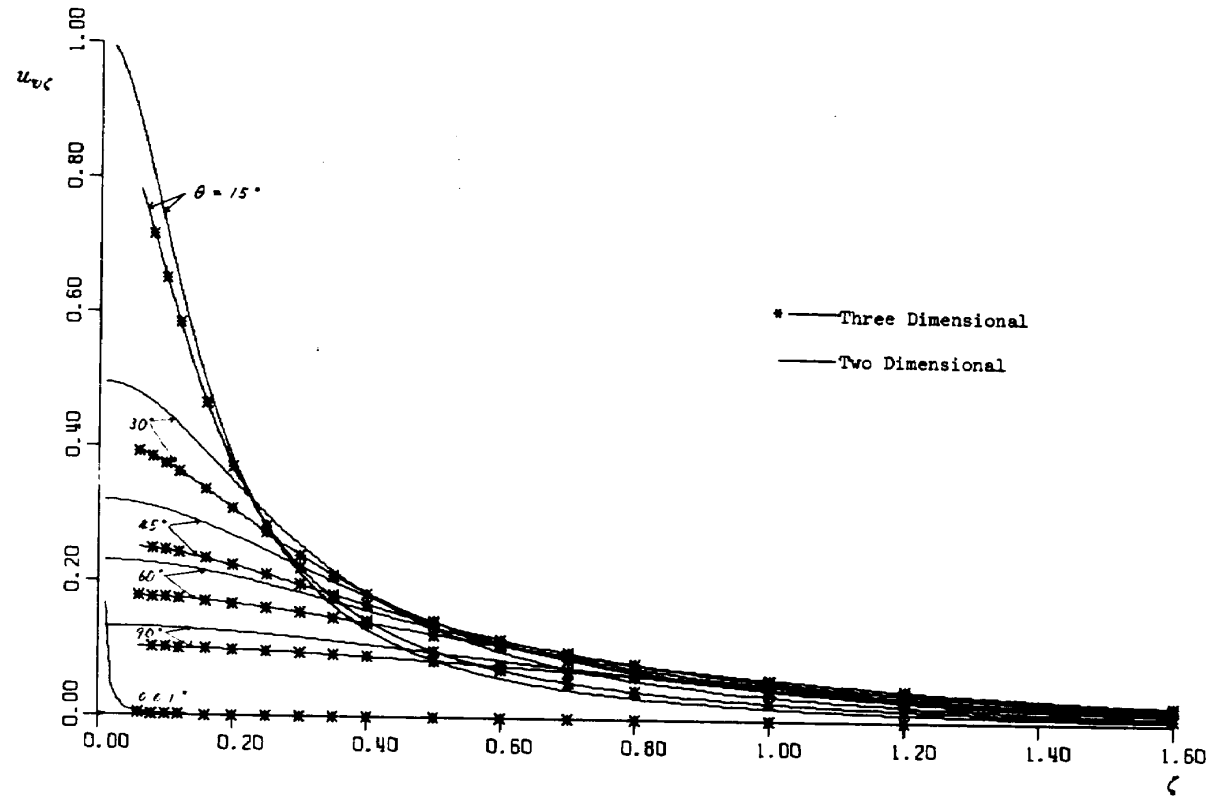

Fig. 9 Axial Velocity Distribution $u_{v\zeta}$ at the Hub(η = 0.6) due to a Single Radial Vortex Line of Strength Unity for ν = 0.6

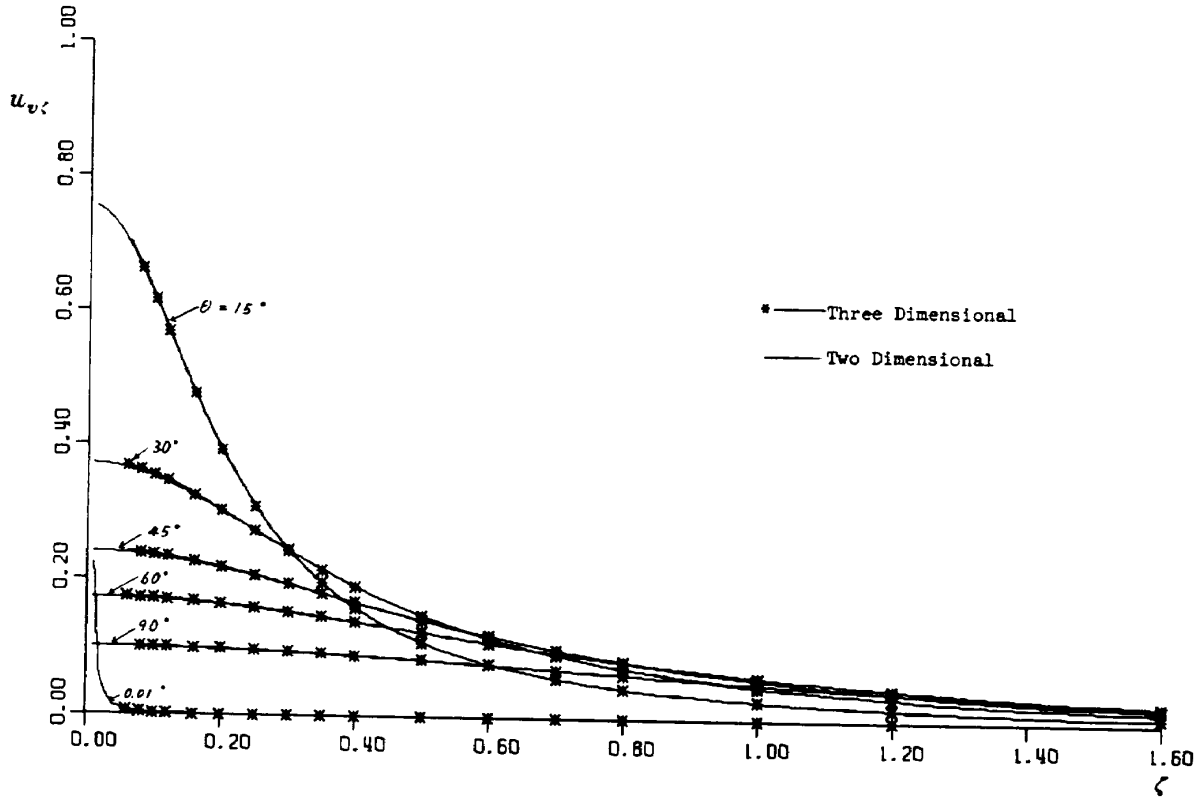

Fig. 10 Axial Velocity Distribution $u_{v\zeta}$ at the Mid Radius(η = 0.8) due to a Single Radial Vortex Line of Strength Unity for ν = 0.6

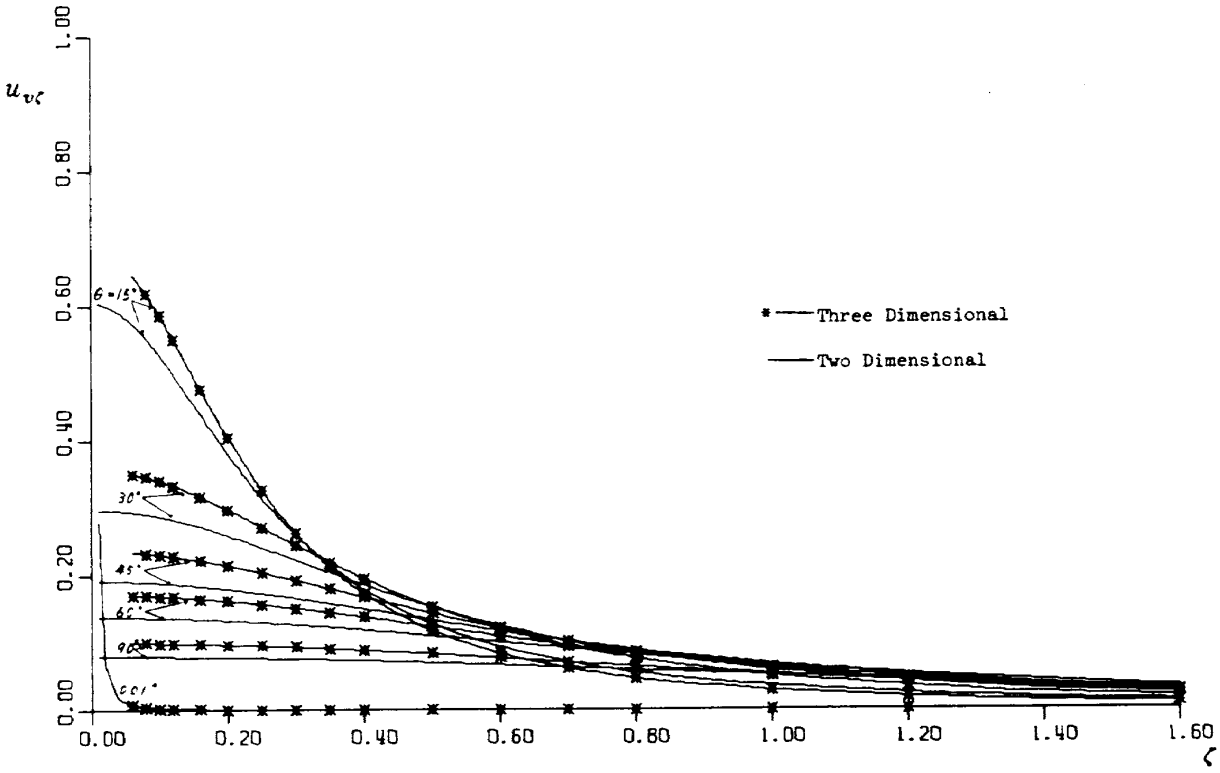

Fig. 11 Axial Velocity Distribution $u_{v\zeta}$ at the Tip(η = 1.0) due to a Single Radial Vortex Line of Strength Unity for ν = 0.6

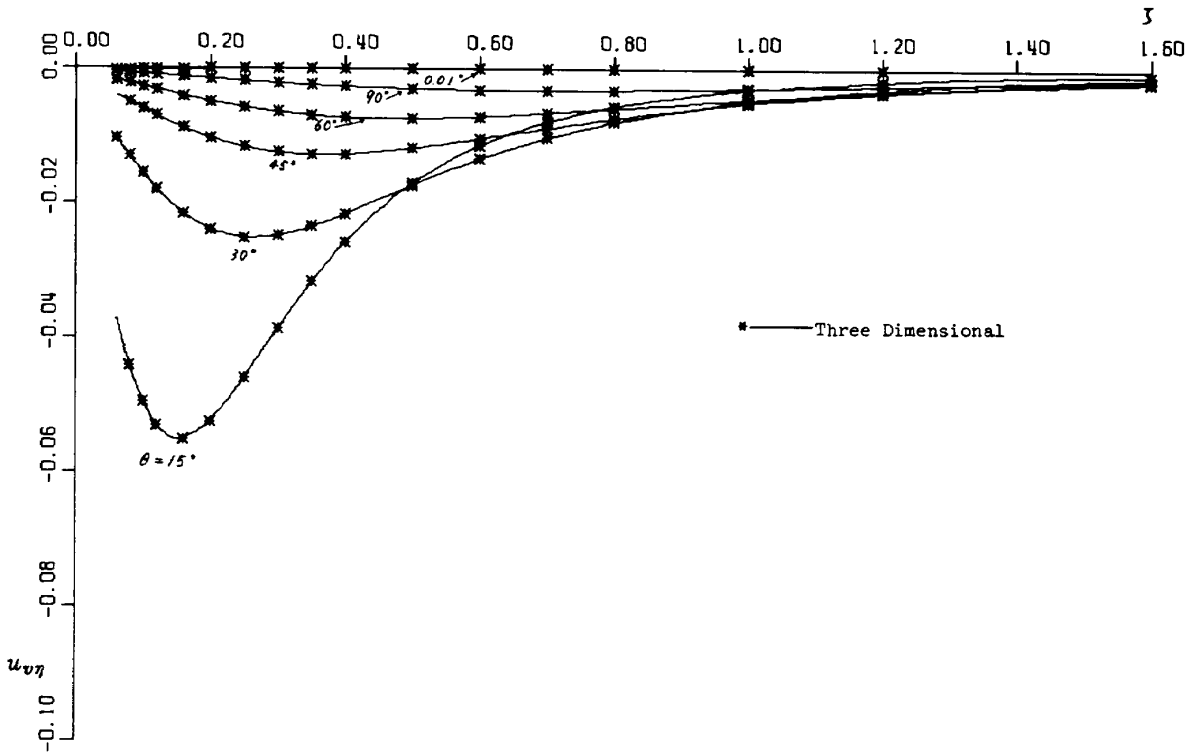

Fig. 12 Radial Velocity Distribution $u_{v\eta}$ at the Mid Radius(η = 0.8) due to a Single Radial Vortex Line of Strength Unity for ν = 0.6

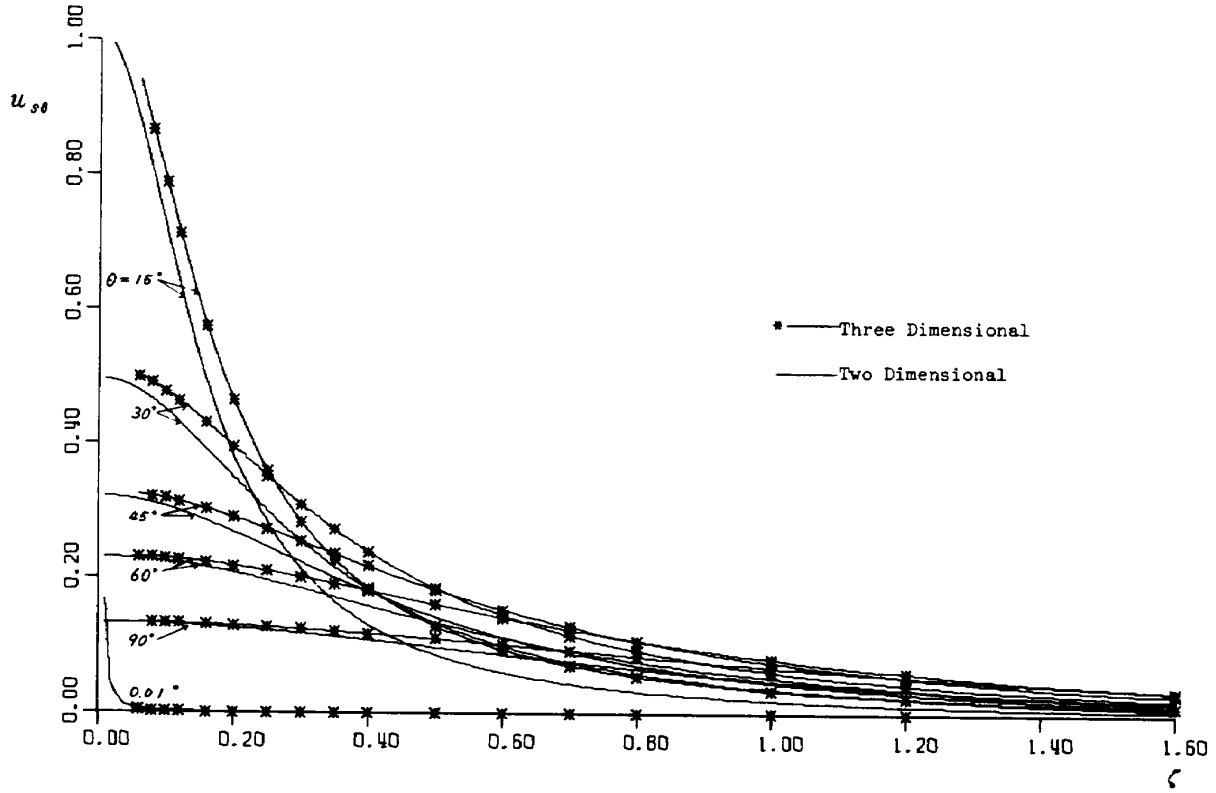

Fig. 13 Tangential Velocity Distribution $u_{s\theta}$ at the Hub(η = 0.6) due to a Single Radial Source Line of Strength Unity for ν = 0.6

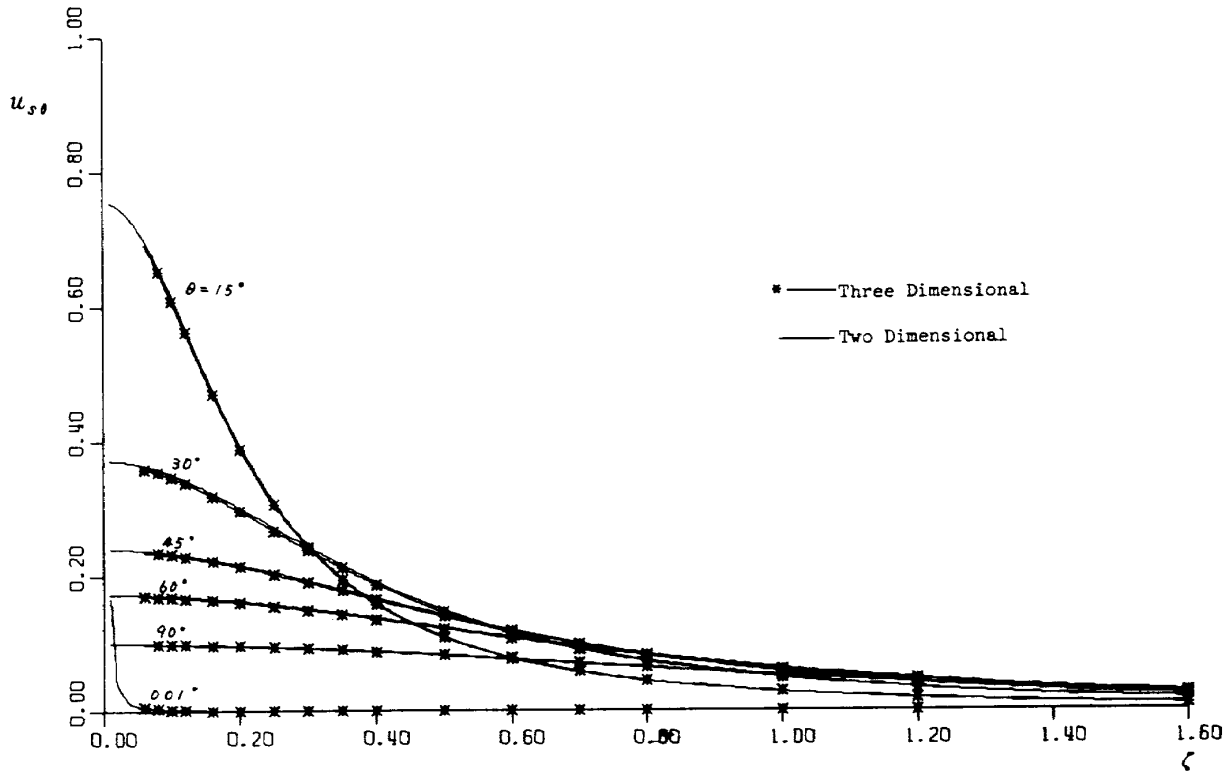

Fig. 14 Tangential Velocity Distribution $u_{s\theta}$ at the Mid Radius(η = 0.8) due to a Single Radial Source Line of Strength Unity for ν = 0.6

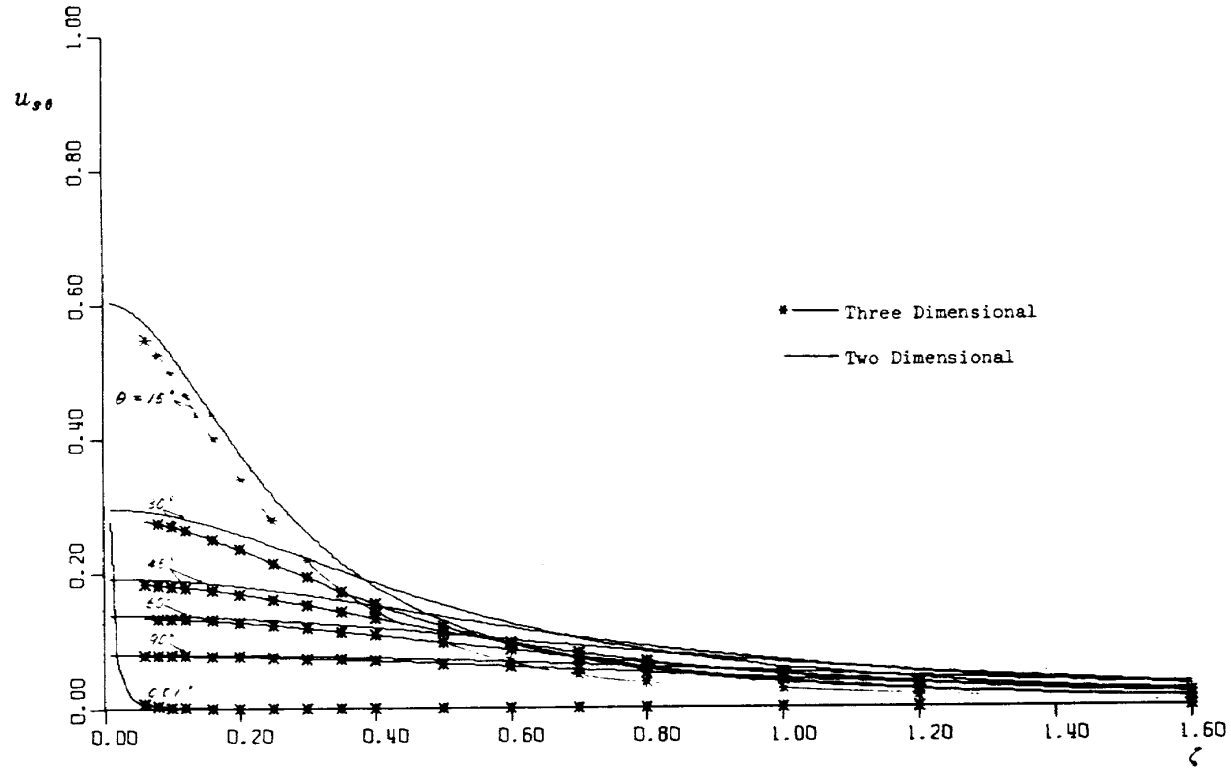

Fig. 15 Tangential Velocity Distribution $u_{s\theta}$ at the Tip(η = 1.0) due to a Single Radial Source Line of Strength Unity for ν = 0.6

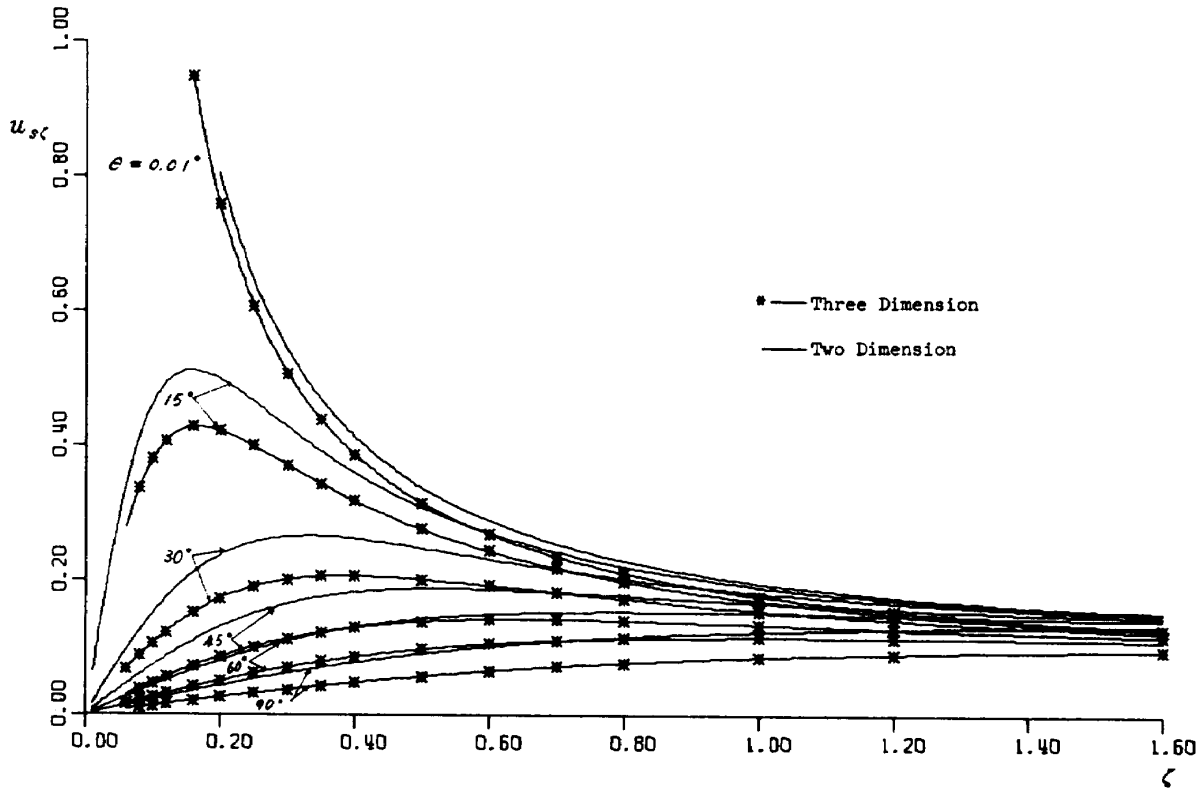

Fig. 16 Axial Velocity Distribution $u_{s\zeta}$ at the Hub(η = 0.6) due to a Single Radial Source Line of Strength Unity for ν = 0.6

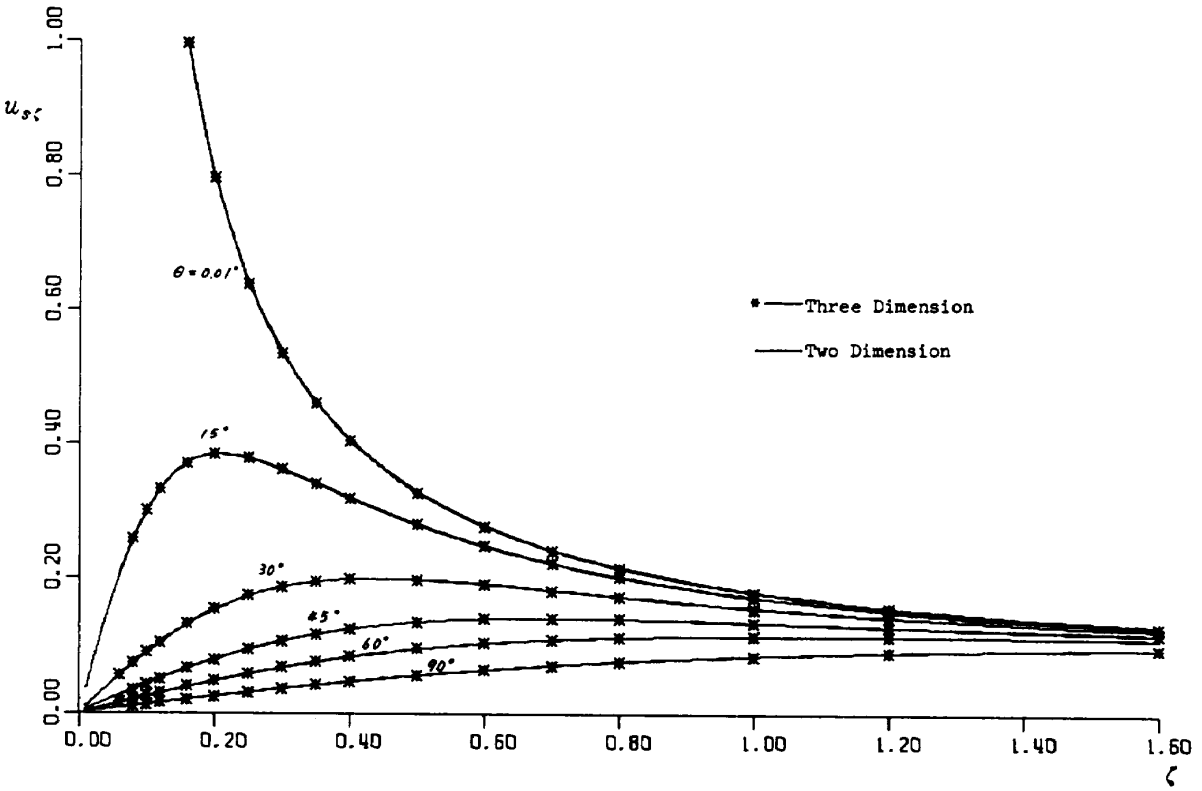

Fig. 17 Axial Velocity Distribution $u_{s\zeta}$ at the Mid Radius(η = 0.8) due to a Single Radial Source Line of Strength Unity for ν = 0.6

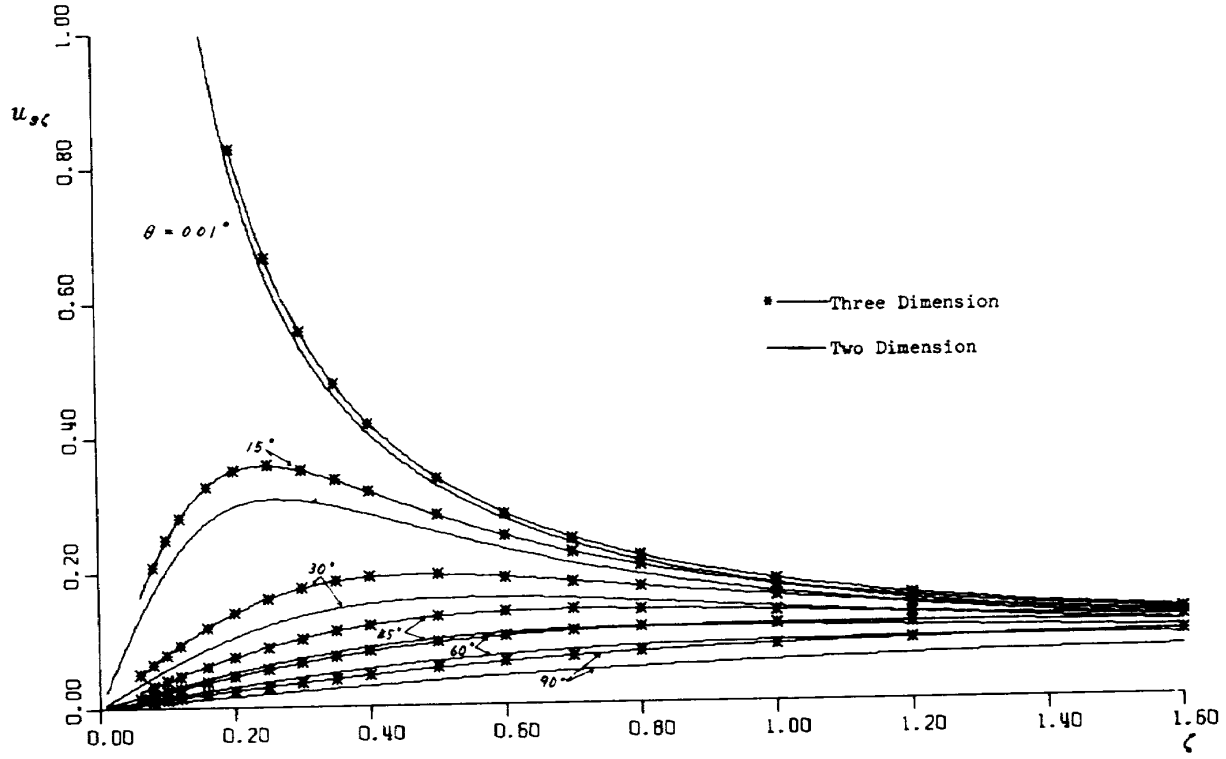

Fig. 18 Axial Velocity Distribution $u_{s\zeta}$ at the Tip(η = 1.0) due to a Single Radial Source Line of Strength Unity for ν = 0.6

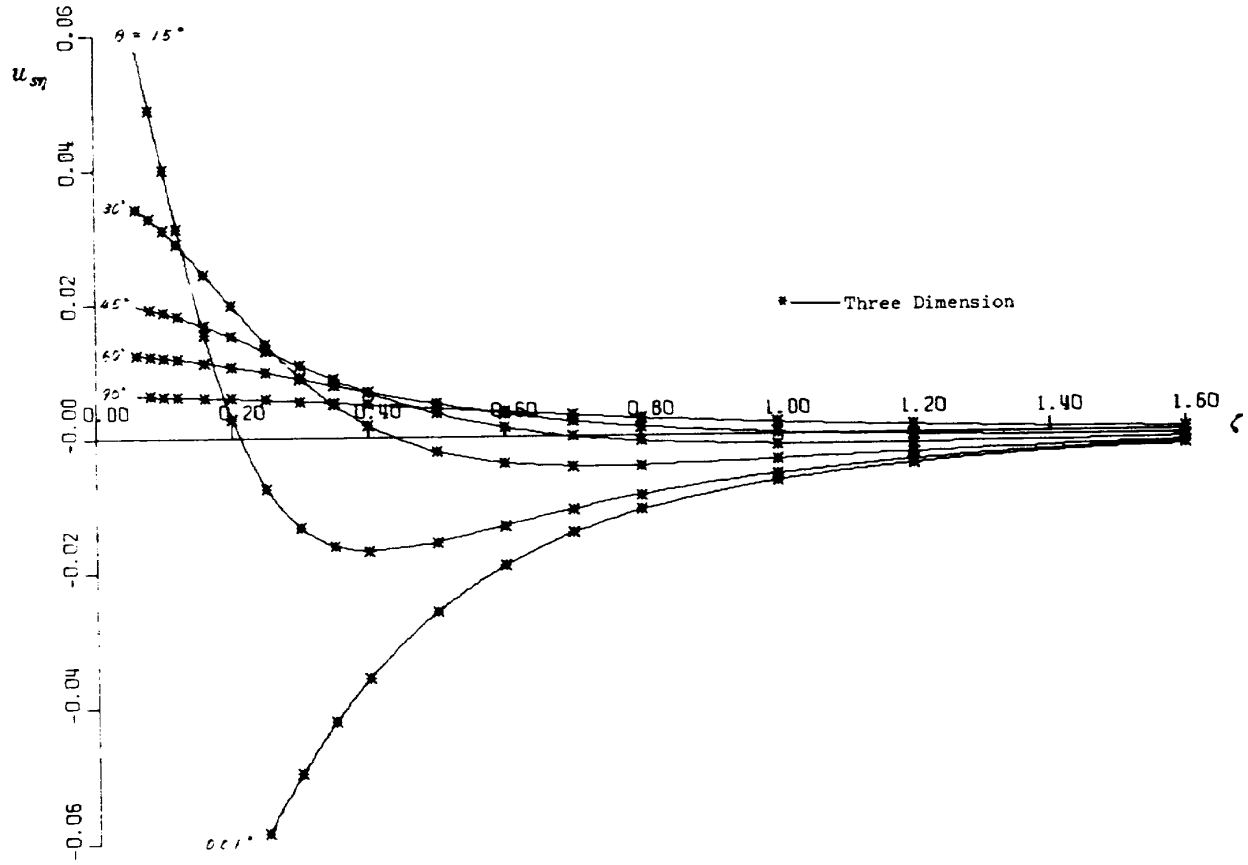

Fig. 19 Fadial Velocity Distribution $u_{s\eta}$ at the Mid Radius(η = 0.8) due to a Single Radial Source Line of Strength Unity for ν = 0.6

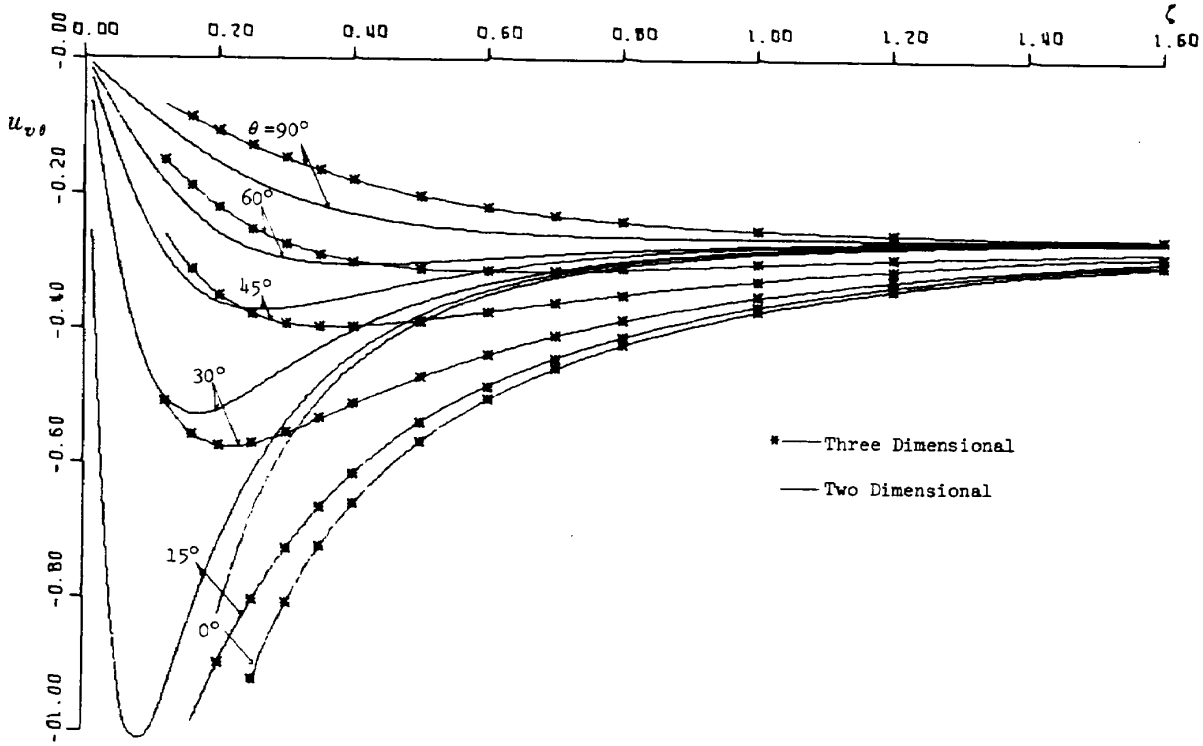

Fig. 20 Tangential Velocity Distribution $u_{v\theta}$ at the Hub(η = 0.3) due to a Single Radial Vortex Line of Strength Unity for ν = 0.3

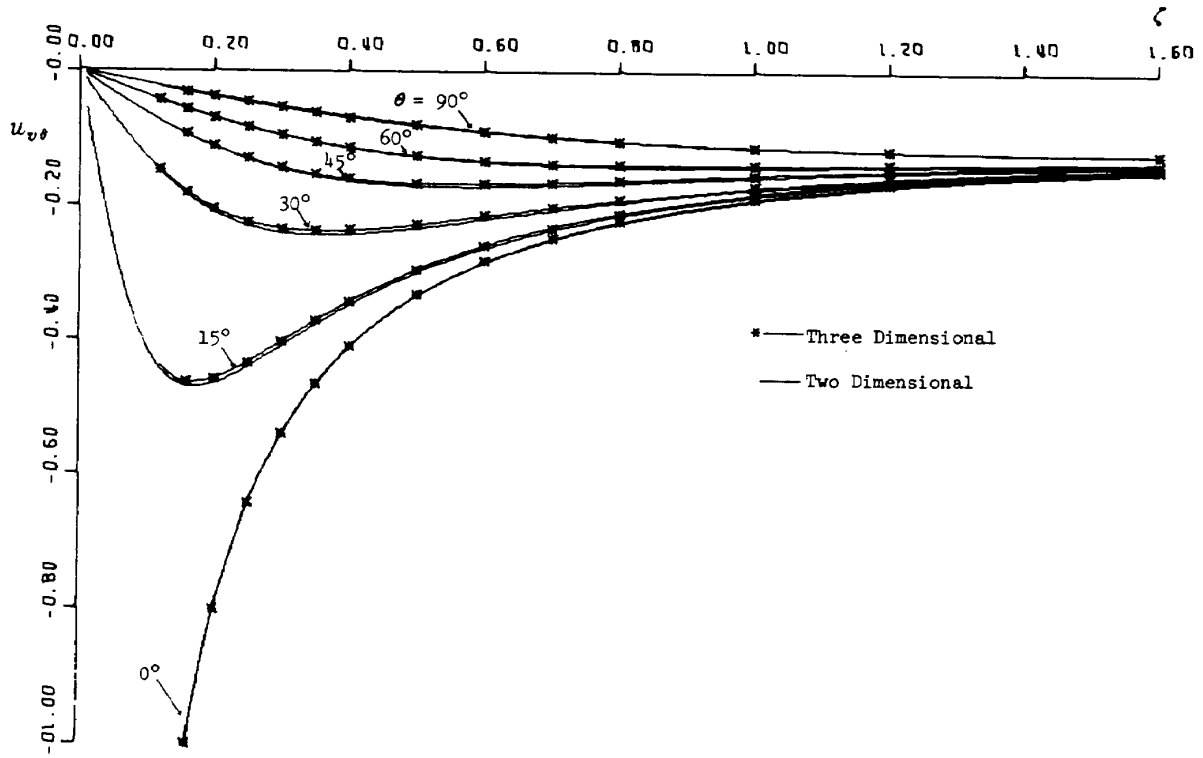

Fig. 21 Tangential Velocity Distribution $u_{v\theta}$ at the Mid Radius(η = 0.65) due to a Single Radial Vortex Line of Strength Unity for ν = 0.3

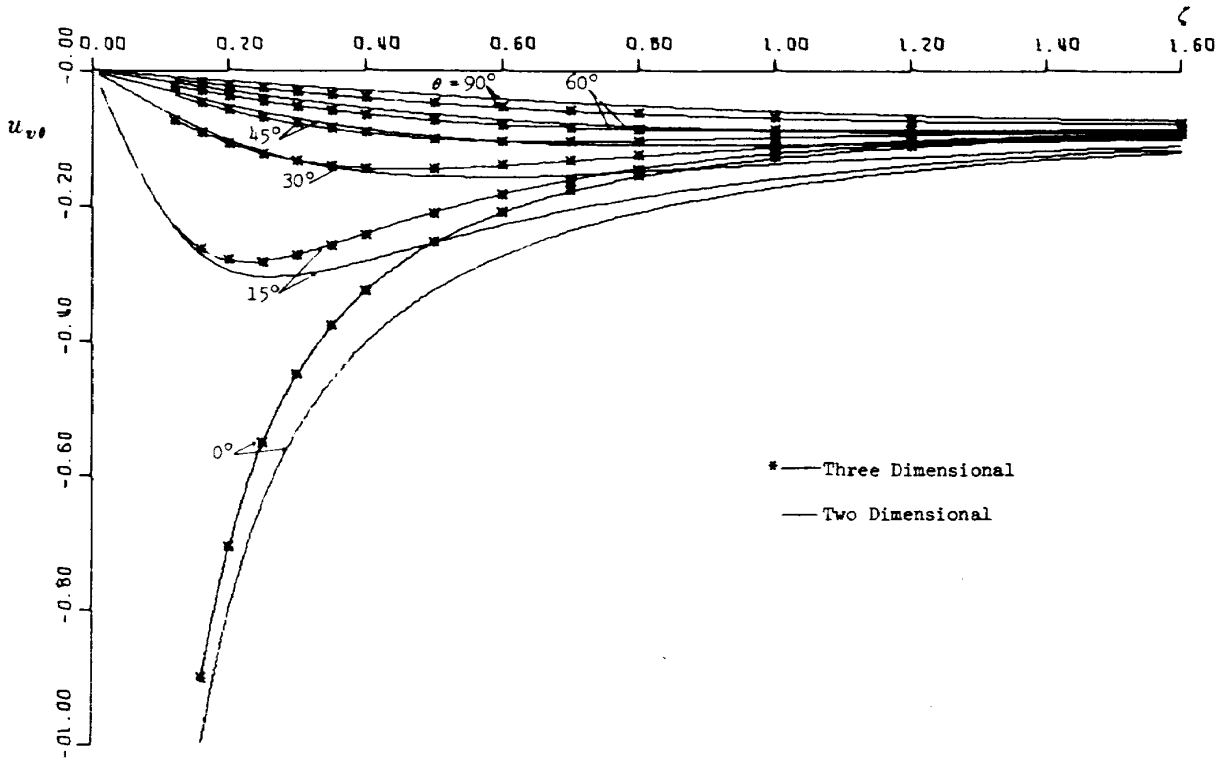

Fig. 22 Tangential Velocity Distribution $u_{v\theta}$ at the Tip(η = 1.0) due to a Single Radial Vortex Line of Strength Unity for ν = 0.3

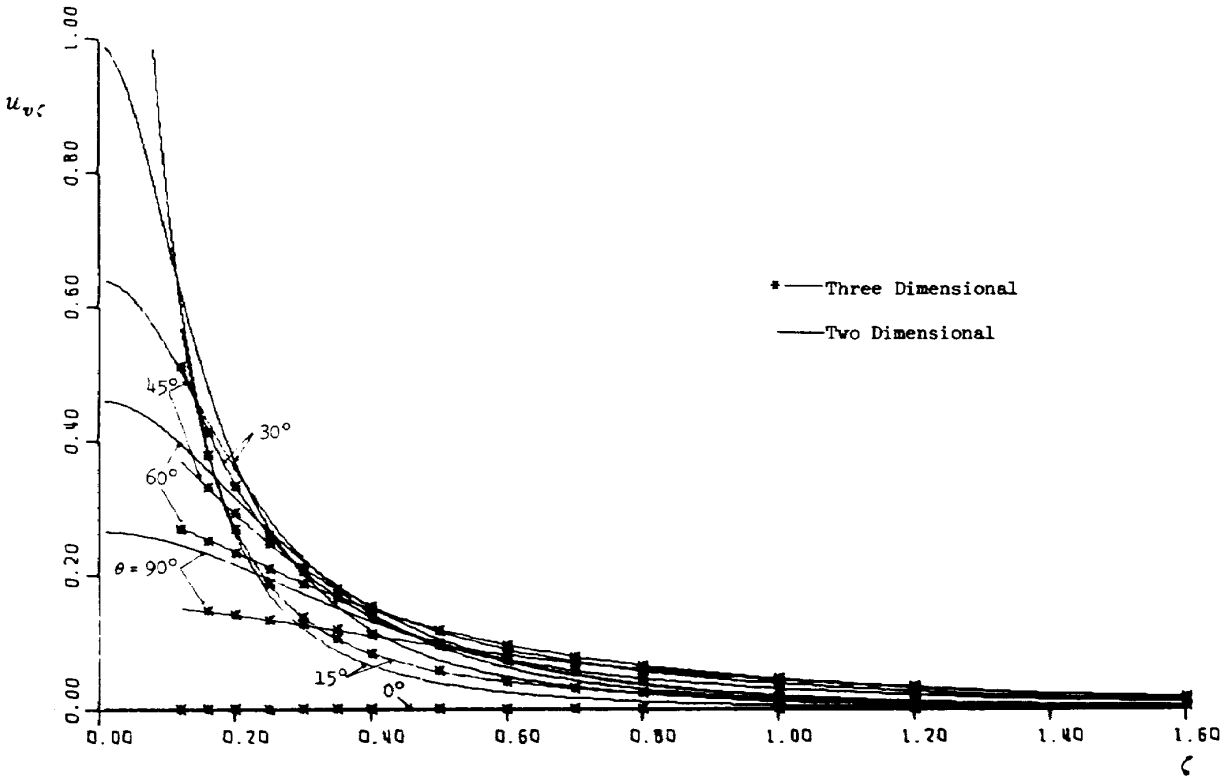

Fig. 23 Axial Velocity Distribution $u_{v\zeta}$ at the Hub(η = 0.3) due to a Single Radial Vortex Line of Strength Unity for ν = 0.3

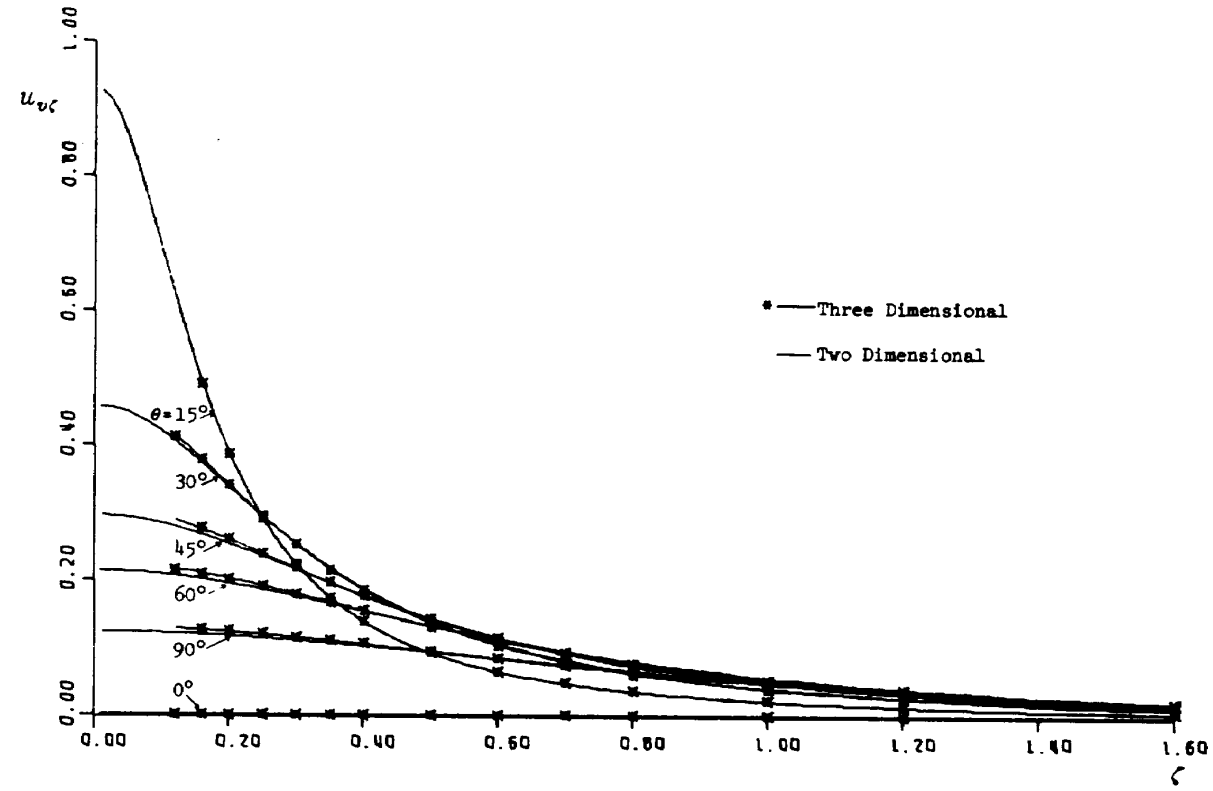

Fig. 24 Axial Velocity Distribution $u_{v\zeta}$ at the Mid Radius(η = 0.65) due to a Single Radial Vortex Line of Strength Unity for ν = 0.3

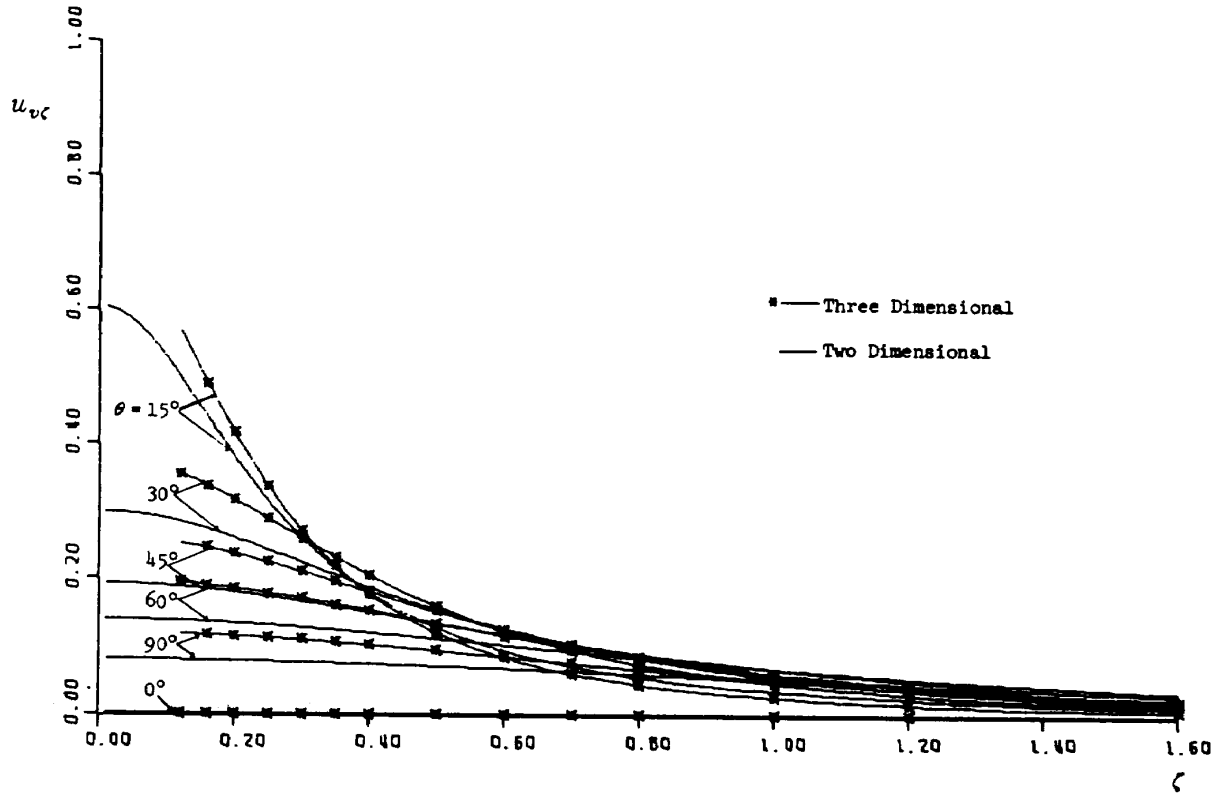

Fig. 25 Axial Velocity Distribution $u_{v\zeta}$ at the Tip(η = 1.0) due to a Single Radial Vortex Line of Strength Unity for ν = 0.3

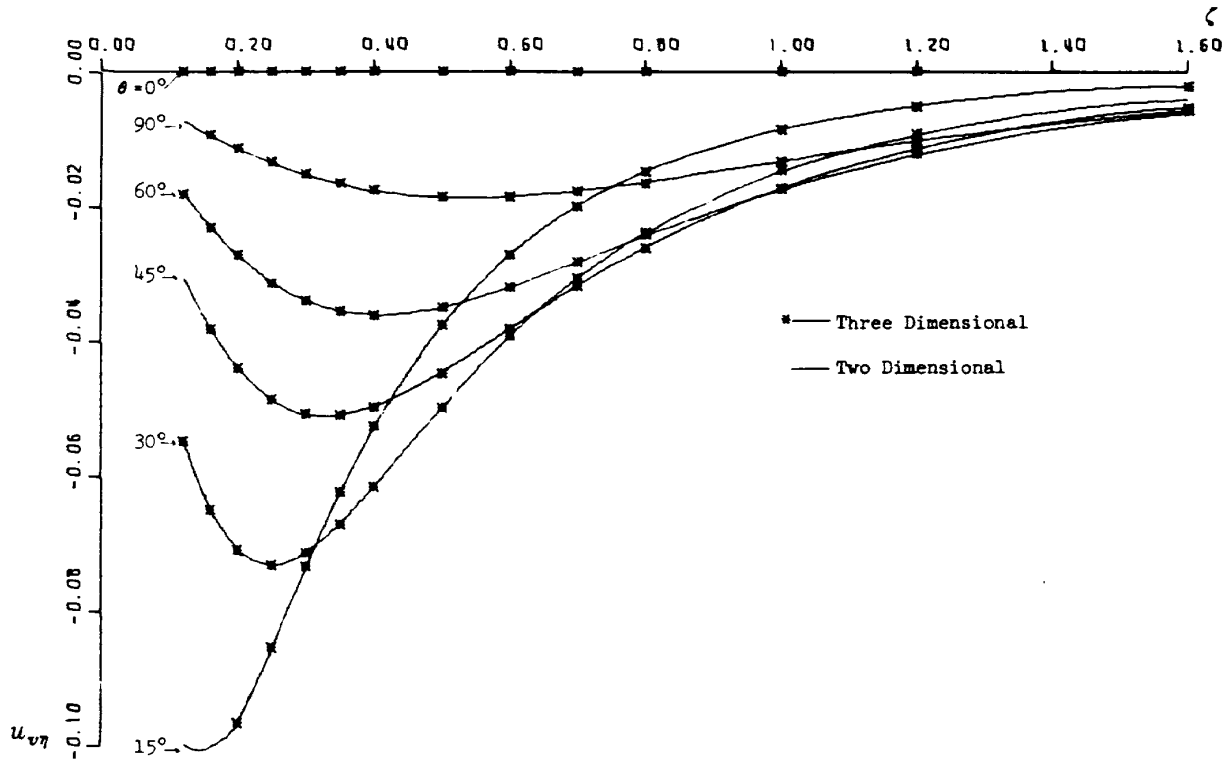

Fig. 26 Radial Velocity Distribution $u_{v\eta}$ at the Mid Radius (η = 0.65) due to a Single Radial Vortex Line of Strength Unity for ν = 0.3

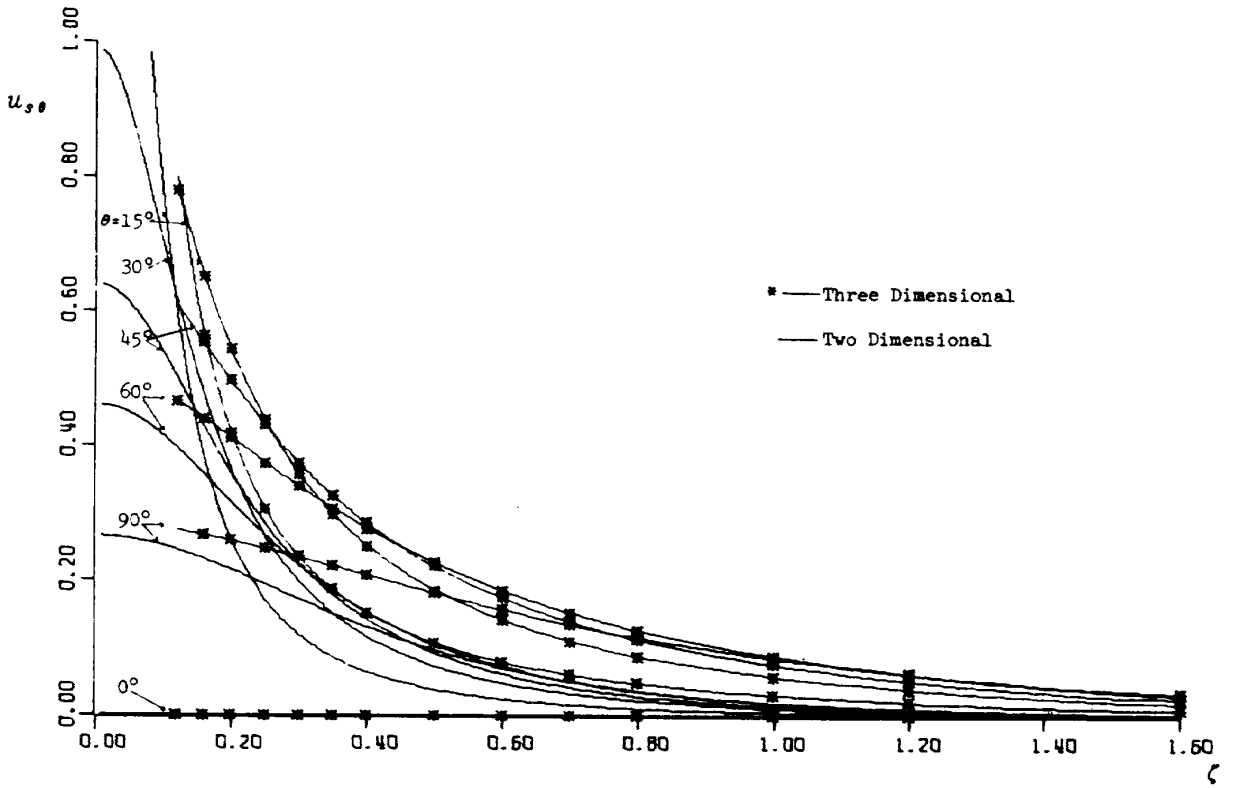

Fig. 27 Tangential Velocity Distribution $u_{s\theta}$ at the Hub(η = 0.3) due to a Single Radial Source Line of Strength Unity for ν = 0.3

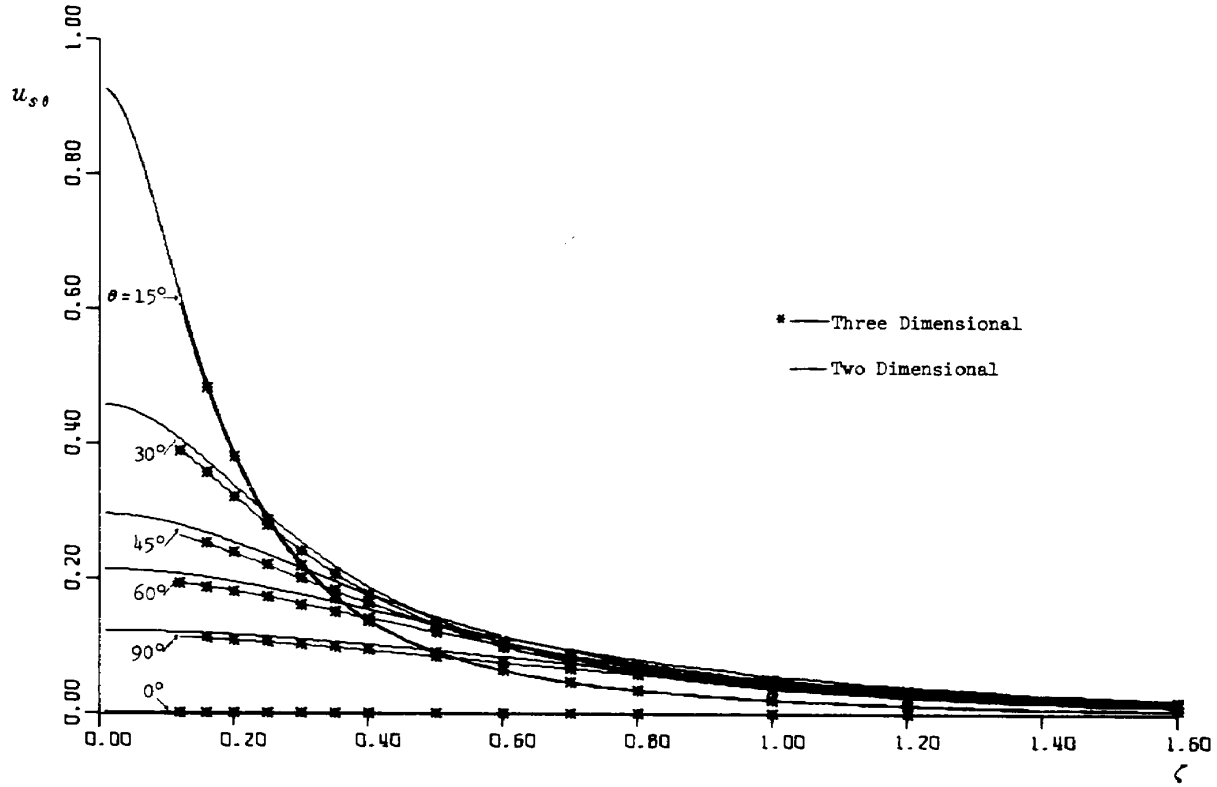

Fig. 28 Tangential Velocity Distribution $u_{s\theta}$ at the Mid Radius(η = 0.65) due to a Single Radial Source Line of Strength Unity for ν = 0.3

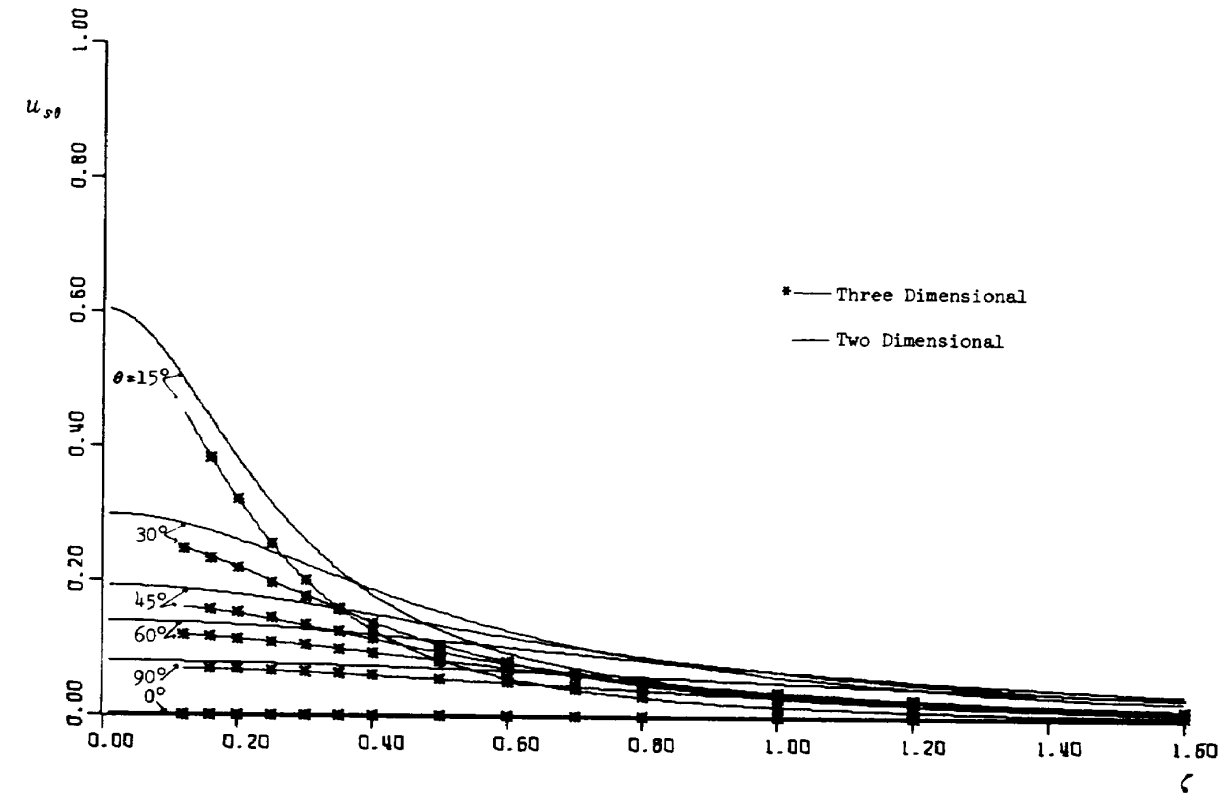

Fig. 29 Tangential Velocity Distribution $u_{s\theta}$ at the Tip(η = 1.0) due to a Single Radial Source Line of Strength Unity for ν = 0.3

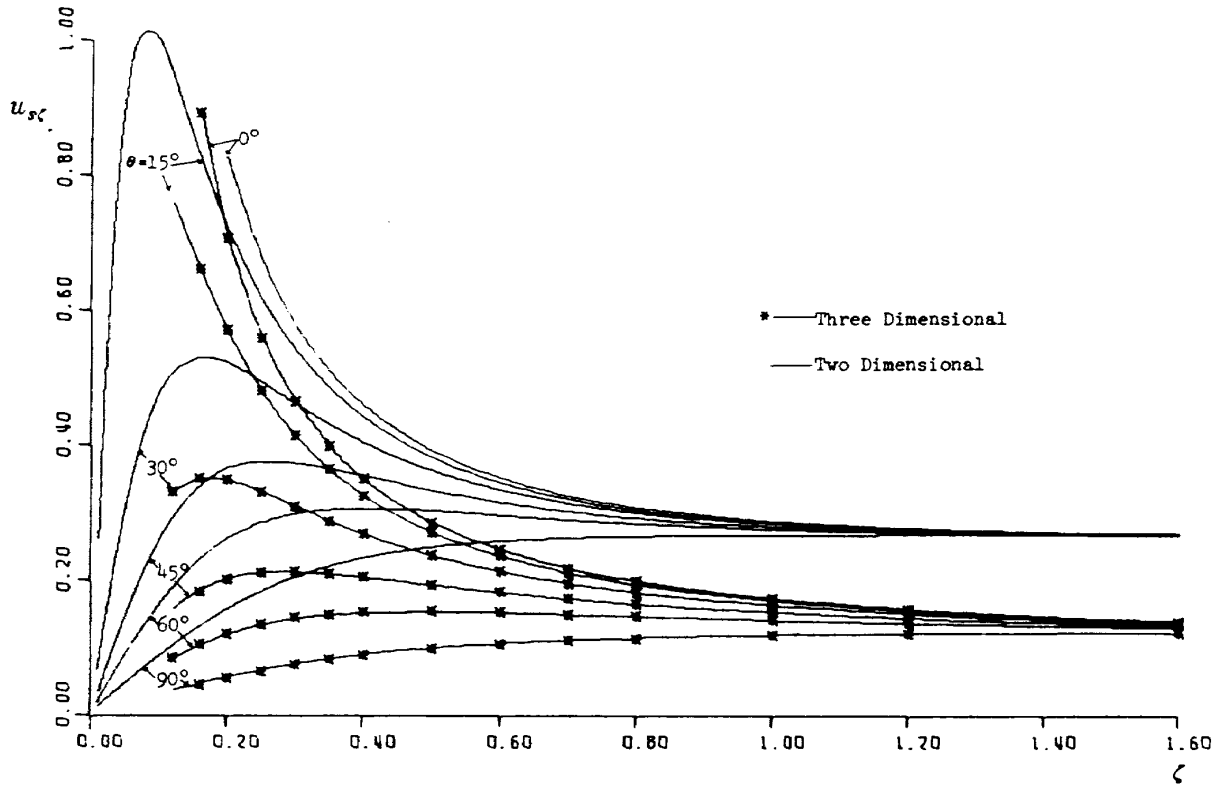

Fig. 30 Axial Velocity Distribution $u_{s\zeta}$ at the Hub(η = 0.3) due to a Single Radial Source Line of Strength Unity for ν = 0.3

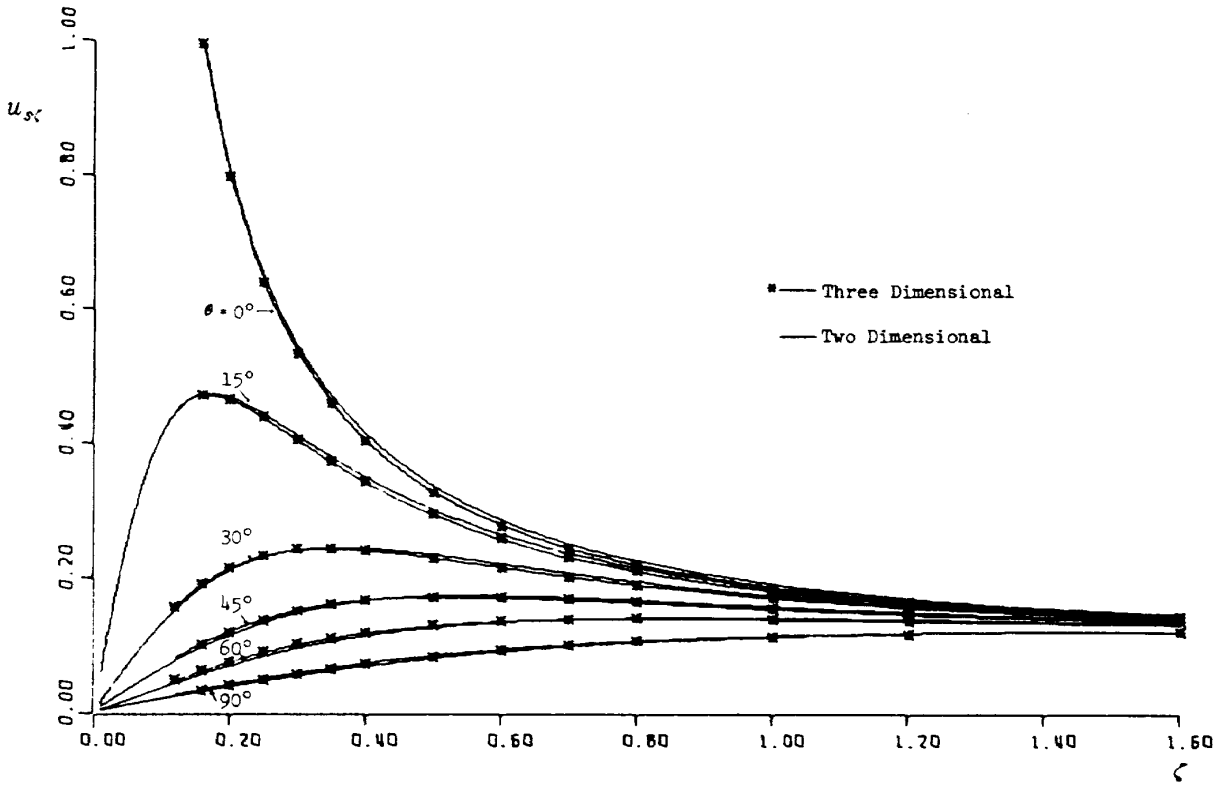

Fig. 31 Axial Velocity Distribution $u_{s\zeta}$ at the Mid Radius (η = 0.65) due to a Single Radial Source Line of Strength Unity for ν = 0.3

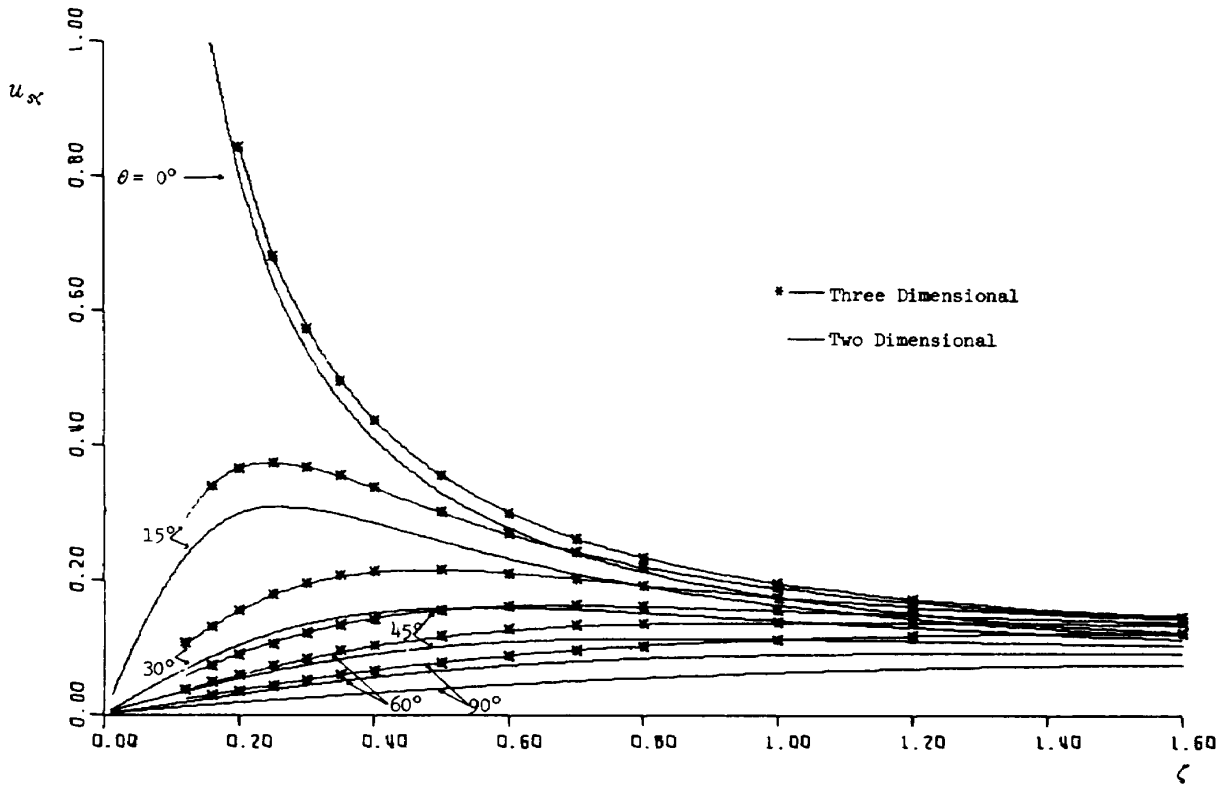

Fig. 32 Axial Velocity Distribution $u_{s\zeta}$ at the Tip(η = 1.0) due to a Single Radial Source Line of Strength Unity for ν = 0.3

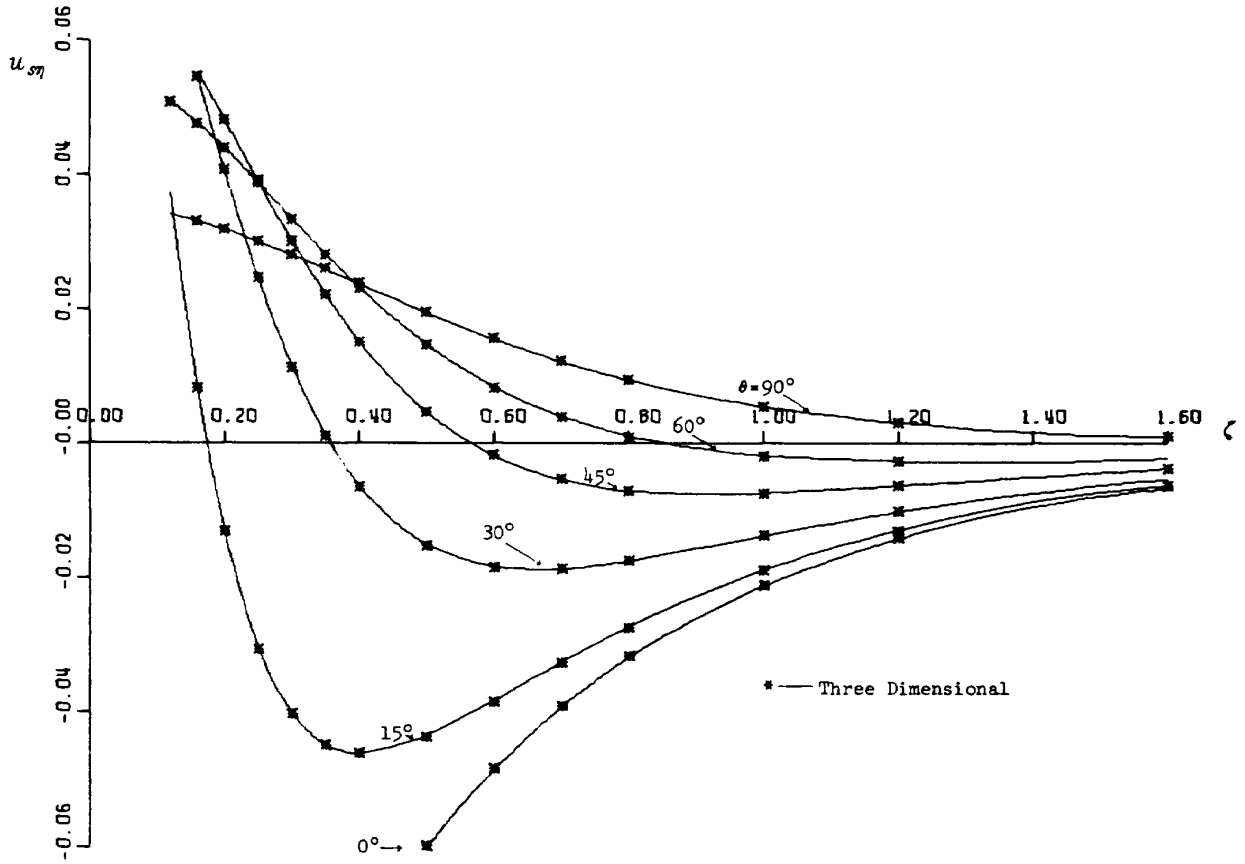

Fig. 33 Radial Velocity Distribution $u_{s\eta}$ at the Mid Radius(η = 0.65) due to a Single Radial Source Line of Strength Unity for ν = 0.3

TECHNICAL REPORT OF NATIONAL
AEROSPACE LABORATORY
TR-378T

航空宇宙技術研究所報告378T号(欧文)

昭和49年8月発行

発行所　航空宇宙技術研究所
東京都調布市深大寺町1,880
電話 武蔵野三鷹(0422)47-5911(大代表)
印刷所　株式会社　共進
東京都杉並区久我山4-1-7(羽田ビル)

Published by
NATIONAL AEROSPACE LABORATORY
1,880 Jindaiji, Chōfu, Tokyo
JAPAN

Printed in Japan